
A DUAL-PAIRING SUMMATION-BY-PARTS FINITE DIFFERENCE FRAMEWORK FOR NONLINEAR CONSERVATION LAWS

A PREPRINT

Kenneth Duru^{3,4}, Dougal Stewart¹, and Nathan Lee²

¹University of Melbourne, Australia

²University of New South Wales, Australia

³Department of Mathematical Sciences, University of Texas at El Paso, USA

⁴Mathematical Sciences Institute, Australian National University, Canberra, Australia

ABSTRACT

Robust and stable high order numerical methods for solving partial differential equations are attractive because they are efficient on modern and next generation hardware architectures. However, the design of provably stable numerical methods for nonlinear hyperbolic conservation laws pose a significant challenge. We present the dual-pairing (DP) and upwind summation-by-parts (SBP) finite difference (FD) framework for accurate and robust numerical approximations of nonlinear conservation laws. The framework has an inbuilt "limiter" whose goal is to detect and effectively resolve regions where the solution is poorly resolved and/or discontinuities are found. The DP SBP FD operators are a dual-pair of backward and forward FD stencils, which together preserve the SBP property. In addition, the DP SBP FD operators are designed to be upwind, that is they come with some innate dissipation everywhere, as opposed to traditional SBP and collocated discontinuous Galerkin spectral element methods which can only induce dissipation through numerical fluxes acting at element interfaces. We combine the DP SBP operators together with skew-symmetric and upwind flux splitting of nonlinear hyperbolic conservation laws. Our semi-discrete approximation is provably entropy-stable for arbitrary nonlinear hyperbolic conservation laws. The framework is high order accurate, provably entropy-stable, convergent, and avoids several pitfalls of current state-of-the-art high order methods. We give specific examples using the in-viscid Burger's equation, nonlinear shallow water equations and compressible Euler equations of gas dynamics. Numerical experiments are presented to verify accuracy and demonstrate the robustness of our numerical framework.

Contents

1	Introduction	2
2	Continuous Analysis	4
2.1	Conservation Laws	4
2.2	Entropy stability	5
2.3	Skew-symmetric splitting	8
3	The SBP finite difference framework for d/dx	11
3.1	Traditional SBP finite difference operators	11
3.2	DP upwind SBP finite difference operators	12

4	Semi-discrete approximation	14
4.1	Finite volume flux splitting and linear stability	15
4.2	The entropy-stable semi-discrete approximation	16
4.3	Numerical conservation properties	18
5	Numerical results	20
5.1	The inviscid Burgers' equation	20
5.2	The shallow water equations	21
5.2.1	Convergence tests for the shallow water equation	21
5.2.2	Well-Balanced	22
5.2.3	The 2D merging vortices	23
5.2.4	Barotropic shear instability	26
5.3	The compressible Euler equations	27
5.3.1	Convergence tests for the 1D compressible Euler equations	29
5.3.2	The 2D isentropic vortex problem	29
5.3.3	Two dimensional Kelvin Helmholtz instability	31
6	Summary and outlook	33
A	2D Shallow Water Equations—Flux Form	37
B	Shallow Water Equations—Vector-Invariant Form	37
C	2D Compressible Euler Equations for an Ideal Gas	38

1 Introduction

Nonlinear hyperbolic conservation laws, defined by systems of nonlinear partial differential equations (PDEs), are widespread in modelling several important physical phenomena and industrial problems such as fluid flow, combustion, black holes, magneto-hydrodynamics, astrophysical and atmospheric fluid dynamics, to name but only a few. Analytical solutions are intractable for most realistic situations. Therefore, accurate and efficient numerical simulations of nonlinear conservation laws are important to academia and industry, and are critical for developing modern technologies, deepening scientific knowledge and paving the way for new inventions and discoveries. The derivation of effective numerical methods for computing approximate solutions of nonlinear conservation laws that are fast, accurate and robust has been a hot research topic beginning from the seminal and early works of von Neumann and Richtmyer [1], Lax and Wendroff [2, 3], Godunov [4], Harten [5], and in recent times has continued to attract substantial interests from the computational and applied mathematics community, see e.g. [6, 7, 8, 9, 10, 11, 12, 13, 14, 15, 16, 17, 18, 19, 20].

Historically, routine numerical approaches to solving nonlinear conservation laws were dominated by low order (first and second order) finite volume and finite difference methods [4, 21, 22, 3] which rely on Godunov-type approximate Riemann solvers. Low order accurate methods can be robust but, because of their inherent excessive numerical dissipation, are not expected to effectively and accurately resolve fine scale and nonlinear features present in the solutions, for example shocks, turbulence, vortices, and highly dispersive wave-dominated phenomena such as gravitational and Rossby wave propagation. High order numerical methods are less dissipative and are known to be efficient and well-suited for wave dominated problems, see e.g., the pioneering work by Kreiss and Oliger [23]. Not all high order methods are acceptable, however, for nonlinear conservation laws.

High order accurate numerical simulations of nonlinear conservation laws are challenging as initial attempts often result in crashes due to compounding numerical errors or the presence of undesirable numerical artefacts which can pollute numerical simulations everywhere. Desirable high order accurate methods for nonlinear hyperbolic conservation laws must be robust (provably stable) and preserve several important invariants present in the system. While

discrete structure preservation of conservation laws and model symmetries of nonlinear conservation laws can improve accuracy, mitigate against numerical instabilities and enhance the robustness of high order numerical approximations, this also introduces additional theoretical and computational demands, such as proof of nonlinear stability, mimetic reformulations and discretizations. In particular, the proof of nonlinear stability for high order numerical methods for systems of nonlinear conservation laws can be technically challenging.

Many previous studies have advocated for numerical methods with provably linear stability, where the assumption of smoothness of solutions is then used to simulate nonlinear problems [24, 25, 26, 27]. However, linearly stable numerical methods are generally not robust for many nonlinear problems and will not yield desirable results in many situations. For instance, turbulence and shocks are highly nonlinear phenomena where linearly stable numerical methods are not sufficient to deliver desirable results. It has been shown and observed in many numerical simulations published in the literature [28, 29, 8, 20], that nonlinear numerical stability is critical to ensuring robustness and accuracy of high order numerical methods for several nonlinear conservation laws. However, before we proceed, first at the continuous level, we must define what it means for a system of nonlinear conservation laws to be nonlinearly stable. We can then mimic the stability properties of the continuous model at the discrete level, leading to a provably nonlinearly stable numerical method.

There are two parallel (and sometimes intersecting) definitions of nonlinear stability, namely, *energy stability* and *entropy stability*. On the one hand, energy stability, which follows from a linear stability theory, aims to bound/conservate a mathematical energy of the solution, a nonnegative functional of the solution (typically a weighted L_2 -norm of the solution for first order systems) at a future time by the energy of the initial (and boundary) data [24, 25, 26, 27, 30, 31, 32]. The energy estimate may sometime coincide with the estimate of the physical energy in the system. However, it is also noteworthy that for certain systems (e.g. Einstein's equations of general relativity) the physical energy is not always nonnegative and may not be useful in deriving nonlinearly stable numerical approximations. On the other hand, an entropy stable numerical method is designed to bound/conservate a mathematical entropy [28, 33, 32, 6, 22, 34, 35, 29, 36, 5], a convex scalar functional that is conserved by the PDE system, for smooth solutions. The notion of entropy stability also has a physical interpretation. For example, a solution of the compressible Euler equations should not only satisfy the nonlinear conservation laws, but also the second law of thermodynamics. A direct implication of this is that the total specific entropy should only increase in a closed system. Consequently, this translates into the solution satisfying an extra partial differential inequality, also known as entropy inequality. A weak solution that satisfies the entropy inequality is considered as the physically correct weak solution [28, 21, 22, 37]. For some systems, such as the Burgers equation and the nonlinear shallow water equations where the energy defines a mathematical entropy, energy stability and entropy stability can be used interchangeably. However, in this paper we will define nonlinear stability in terms of entropy stability. That is, a system of nonlinear conservation laws is entropy stable if there is a mathematical entropy which is conserved by the system for smooth solutions.

For an entropy stable system of PDEs, a provably nonlinearly stable numerical method can be derived by replicating the continuous analysis at the discrete level. An essential ingredient for the development of provably stable numerical methods for PDEs is the summation-by-parts (SBP) principle [38, 39, 40, 41, 42, 43], with its mimetic structure, which allows provably stable methods to be constructed at the semi-discrete level, as long as careful numerical treatments of the boundary conditions are provided. At the continuous level, however, the key ingredients that are necessary in proving stability results are integration by parts, and possibly the chain rule and the product rule. So, while SBP numerical derivative operators are designed to mimic integration by parts property at the discrete level, it is challenging for SBP operators to mimic the chain rule or product rule at the discrete level. To be able to replicate the continuous analysis at the discrete level, the system of nonlinear conservation laws at the continuous level must be rewritten into the so-called skew-symmetric or entropy-conserving split-form so that we can negate the use of the chain rule and product rule at the discrete level. For standard systems of nonlinear conservation laws there are several artful ways of doing this, see e.g. [6, 7, 8, 9, 44, 45, 20, 15, 14, 30]. We note, however, for several systems of PDEs finding a mathematical entropy and the skew-symmetric formulation that can be targeted by SBP discretizations can be cumbersome and nontrivial.

Once an entropy functional is identified and an entropy conserving or mimetic reformulation of the PDE system is given, then the system can be approximated by SBP operators leading to an entropy conserving numerical method. While, theoretically, this may yield a provably nonlinearly stable numerical method, however, traditional SBP operator for the first derivative based central FD stencils [38, 39, 40, 41] or collocated discontinuous Galerkin spectral element method (DG-SEM) [42, 43, 14] can suffer from spurious unresolved wave-modes, which can destroy the accuracy of numerical solutions and crash the simulation of a nonlinear conservation law. It was recently shown in [29] that the local linear stability property of high order methods is necessary for convergent numerical simulations of nonlinear conservation laws. Sadly, state-of-the-art high order accurate SBP FD and DG-SEM entropy stable schemes for nonlinear conservation in skew-symmetric split form are not locally energy stable, and do not satisfy this necessary criterion. Therefore, a sufficient amount of dissipation must be added, by filtering, limiting or artificial numerical

dissipation, to stabilize the simulation and obtain acceptable results. Numerical dissipation helps in many ways, but it can lower numerical accuracy, compromise the conservative properties of the system and introduce interesting and undesirable numerical artefacts. In this study we propose a new high order accurate and provably nonlinearly stable numerical framework for nonlinear conservation laws that significantly minimizes oscillations from shocks and avoids several pitfalls of current state-of-the-art high order methods. We are currently investigating the local energy-stability properties of the proposed DP SBP framework and comparing with other high-order schemes. The results of these will be reported in our forthcoming paper.

The dual-pairing (DP) SBP framework [46, 47, 48] was recently introduced to improve the accuracy of FD methods for wave problems and nonlinear conservation laws, in complex geometries. The DP-SBP operators are a pair of high order (backward and forward) difference stencils which together preserve the SBP principle. The DP-SBP operators also have additional degrees of freedom which can be tuned to diminish numerical dispersion errors, yielding the so-called dispersion-relation-preserving (DRP) DP-SBP FD operators [48]. However, the DP-SBP operators are asymmetric and dissipative, can potentially destroy symmetries that exist in the continuum problem. To obtain acceptable results, the DP-SBP operators must be combined in a careful manner so that we can prove numerical stability and preserve model symmetries. Recent applications of DP-SBP operators to nonlinear conservation laws [49, 50] combines the operators with classical finite volume flux splitting [21, 4, 22] so that the upwind features of DP-SBP operators induces some dissipation. The resulting numerical methods [49, 50] are provably linearly stable. As we have recounted linear stability is not sufficient to simulate highly nonlinear phenomena such as turbulence. This is corroborated by the numerical experiments of turbulent flows performed later in this paper and in [49] for linearly stable methods using the DP-SBP operators, where the simulations of the classical Kelvin-Helmholtz instability crashed when the flow became turbulent.

In this paper we present the DP upwind SBP FD framework for efficient, accurate and robust numerical approximations of nonlinear conservation laws. The DP SBP FD operators are designed to be upwind, that is they come with some built-in dissipation everywhere, as opposed to DG-SEM which can only induce dissipation through numerical fluxes acting at element interfaces. We combine the DP SBP operators together with skew-symmetric and upwind flux splitting of nonlinear hyperbolic conservation laws. The semi-discrete approximation is conservative and provably entropy-stable for arbitrary nonlinear hyperbolic conservation laws. That is, for smooth solutions it conserves entropy and dissipates entropy when solutions are non-smooth. We give specific examples using the in-viscid Burger's equation, nonlinear shallow water equations and compressible Euler equations of gas dynamics. We focus primarily on initial value problems (IVP) driven by initial conditions or internal forcing with periodic boundary conditions. Extensive and detailed numerical experiments are presented verifying accuracy, stability and the conservative properties of the method. Long time numerical simulations of merging vortices, barotropic shear instability and the Kelvin-Helmholtz instability, with fully developed turbulence, demonstrate the robustness and accuracy of the framework when compared with the state-of-the-art methods.

The rest of the paper is organised as follows. In Section 2 we perform the continuous analysis, give a quick review of skew-symmetric and entropy conserving flux splitting of nonlinear conservation laws. Next, in section 3, we introduce the SBP FD framework for first derivative d/dx and detail the necessary assumptions that define the traditional SBP framework [38, 39] and the DP upwind SBP framework [46, 47, 48]. In section 4 we derive the semi-discrete approximations for an arbitrary conservation and prove the conservative and stability properties of the numerical framework. In section 5 we present detailed numerical experiments verifying accuracy, discrete conservative and stability properties, and the robustness of the proposed method. Section 6 summarises the results of the study and speculates on the direction of future research.

2 Continuous Analysis

In this section we present and analyze the model problems. We perform entropy stability analysis and present the skew-symmetric reformulations of the model problems.

2.1 Conservation Laws

We are concerned with the numerical approximation of solutions $\mathbf{u}(\mathbf{x}, t) \in \mathbb{R}^m$ to PDEs of the form

$$\partial_t \mathbf{u}(\mathbf{x}, t) + \nabla \cdot \mathbf{f}(\mathbf{u}(\mathbf{x}, t)) = 0, \quad \mathbf{x} \in \Omega \subset \mathbb{R}^d, \quad t \in [0, T], \quad (1)$$

where $\mathbf{u} : \Omega \times [0, T] \rightarrow \mathbb{R}^m$ with $m \geq 1$ is the unknown solution, $\mathbf{f} : \mathbb{R}^m \rightarrow \mathbb{R}^{m \times d}$ is the flux function of the PDE, $d \geq 1$ denotes the spatial dimension, $\mathbf{x} = (x_1, x_2, \dots, x_d) \in \mathbb{R}^d$ is the spatial variable and $t \in [0, T]$ denotes time and $T > 0$ is the final time. We set the smooth initial condition $\mathbf{u}(\mathbf{x}, 0) = \mathbf{u}_0(\mathbf{x}) \in C^1(\Omega)$. Such PDEs are known as conservation laws and often appear in science and engineering where \mathbf{u} is a set of conserved variables which

may denote some physical quantity such as velocity, momentum, mass, pressure, density, energy, magnetic/electric field, etc. Conservation laws are aptly named because they state that the total quantity of \mathbf{u} is conserved. This can be understood by integrating (1) and then applying the divergence theorem,

$$\partial_t \mathcal{U}(t) = - \oint_{\partial\Omega} \mathbf{f}(\mathbf{u}(\mathbf{x}, t)) \cdot \mathbf{n} \, d\mathbf{x}, \quad \mathcal{U}(t) = \int_{\Omega} \mathbf{u}(\mathbf{x}, t). \quad (2)$$

That is, a conservation law essentially states that the change in the total quantity $\mathcal{U}(t)$ in any given region of space Ω is governed by the flux $\mathbf{f}(\mathbf{u}) \cdot \mathbf{n}$ going in and out of the boundary $\partial\Omega$, where \mathbf{n} is the outward unit normal on the boundary. In particular, for continuous periodic solutions in Ω the total quantity $\mathcal{U}(t)$ is conserved, that is $\partial_t \mathcal{U}(t) = 0$ for all $t \geq 0$. For nonlinear hyperbolic conservation laws with weak solutions, the conservative properties of a numerical method is critical for the convergence of numerical solutions [3].

By using the chain rule and the product rule we can rewrite the nonlinear conservation (1) in the quasilinear form

$$\partial_t \mathbf{u} + \sum_{\nu=1}^m A_{x_\nu} \frac{\partial \mathbf{u}}{\partial x_\nu} = 0, \quad A_{x_\nu} \in \mathbb{R}^{m \times m}, \quad t \in [0, T], \quad (3)$$

where the square matrices $A_{x_\nu}(\mathbf{u}) = \partial_{\mathbf{u}} \mathbf{f}_\nu$, for $\nu = 1, 2, \dots, d$, are the Jacobian of the flux. We are particularly interested in nonlinear strongly hyperbolic conservation laws. This is equivalent to the matrix $A = \sum_{\nu=1}^d k_\nu A_{x_\nu}$, with $\sum_{\nu=1}^d k_\nu^2 = 1$, being diagonalisable with real eigenvalues [51] for all admissible state $\mathbf{u} \in \mathbb{R}^m$.

In this work, we will focus on initial value problems (IVP) driven by initial conditions or internal forcing for systems of nonlinear hyperbolic conservation laws. We will typically consider one and two space dimensions ($d = 1, 2$) and assume periodic boundaries such that the boundary integral in the right-hand side of (2) vanishes. However, our framework can be extended arbitrary number of space dimensions. Well-posed non-periodic boundary conditions can be implemented, for example using the SAT method [52, 53, 10, 35]. That said, it is also important to note that numerical treatments of boundary conditions is problem specific and come with additional theoretical and practical difficulties, in particular for nonlinear conservation laws. Therefore, the formulation of well-posed boundary conditions for nonlinear conservation laws and their numerical treatments are beyond the scope of the present study.

2.2 Entropy stability

An interesting phenomena that occurs with hyperbolic nonlinear conservation laws are discontinuities that develop in the solution as it evolves, even if start with smooth initial conditions. Such discontinuities such as shocks and contact discontinuities can be problematic because partial derivatives are not well defined for discontinuities. Instead, one can consider weak solutions of the IVP [37, 2, 21], where some notion of a *weak* derivative can make sense. Unfortunately, there can exist multiple weak solutions, and so we must impose at least one additional condition to define a unique solution. One criterion used is known as an entropy inequality, which uniquely chooses the so-called vanishing-viscosity solution. For gas dynamics, this is considered as the physically correct weak solution [28, 21, 22, 37].

We introduce the L_2 inner product and norm

$$(\mathbf{u}, \mathbf{v}) = \int_{\Omega} \mathbf{u}^\top \mathbf{v} \, d\mathbf{x}, \quad \|\mathbf{u}\|^2 = (\mathbf{u}, \mathbf{u}). \quad (4)$$

We define an entropy pair e, \mathbf{q} , with $e : \mathbb{R}^m \rightarrow \mathbb{R}$, $\mathbf{q} : \mathbb{R}^m \rightarrow \mathbb{R}^d$, where $e(\mathbf{u})$ is called the entropy function, and $q(\mathbf{u})$ satisfying $\partial_{\mathbf{u}} \mathbf{q}(\mathbf{u}) = \mathbf{g}^\top \partial_{\mathbf{u}} \mathbf{f}(\mathbf{u})$ is called the entropy flux, where $\mathbf{g} : \mathbb{R} \rightarrow \mathbb{R}^m$ with $\mathbf{g} = \partial_{\mathbf{u}} e(\mathbf{u})$ are the entropy variables. In addition, we may require that the entropy $e(\mathbf{u})$ is convex, that is the hessian $H_{\mathbf{u}}(e(\mathbf{u})) \in \mathbb{R}^{m \times m}$ is positive semi-definite. In the case that \mathbf{u} is smooth we multiply (1) by \mathbf{g}^\top and apply the chain rule, we have

$$\mathbf{g}^\top \partial_t \mathbf{u} + \mathbf{g}^\top \nabla \cdot \mathbf{f}(\mathbf{u}) = 0 \iff \mathbf{g}^\top \partial_t \mathbf{u} + \mathbf{g}^\top \partial_{\mathbf{u}} \mathbf{f}(\mathbf{u}) \cdot \partial_{\mathbf{x}} \mathbf{u} = 0.$$

Note that $\partial_{\mathbf{u}} \mathbf{f}(\mathbf{u}) : \mathbb{R}^{m \times d} \rightarrow \mathbb{R}^{m \times d \times m}$ and $\partial_{\mathbf{x}} \mathbf{u} : \mathbb{R}^m \rightarrow \mathbb{R}^{m \times d}$ are tensors. Using the fact $\partial_{\mathbf{u}} \mathbf{q}(\mathbf{u}) = \mathbf{g}^\top \partial_{\mathbf{u}} \mathbf{f}(\mathbf{u})$ and reversing the chain rule in time and space giving

$$\partial_t e + \nabla \cdot \mathbf{q} = 0. \quad (5)$$

Indeed, the entropy e satisfies a conservation law. That is, the total entropy

$$E(t) := (1, e) = \int_{\Omega} e(\mathbf{u}(\mathbf{x}, t)) \, d\mathbf{x}, \quad (6)$$

is conserved for smooth periodic solutions,

$$\frac{d}{dt}E(t) = \frac{d}{dt} \int_{\Omega} e(\mathbf{u}(\mathbf{x}, t)) d\mathbf{x} = - \oint_{\partial\Omega} \mathbf{q} \cdot \mathbf{n} d\mathbf{x} = 0. \quad (7)$$

However, when \mathbf{u} is discontinuous we may impose the entropy inequality, which states that the entropy solution \mathbf{u} must weakly satisfy the inequality [28, 22]

$$\partial_t e + \nabla \cdot \mathbf{q} \leq 0, \quad (8)$$

for all entropy pairs e, \mathbf{q} with convex entropy function e . Clearly, the local entropy inequality (8) implies that total entropy at any future time is bounded by the initial total entropy, that is

$$\frac{d}{dt}E(t) = \frac{d}{dt} \int_{\Omega} e(\mathbf{u}(\mathbf{x}, t)) d\mathbf{x} \leq - \oint_{\partial\Omega} \mathbf{q} \cdot \mathbf{n} d\mathbf{x} = 0 \iff E(t) \leq E(0), \quad \forall t \geq 0. \quad (9)$$

When \mathbf{u} is sufficiently smooth we have equality as shown earlier. For more elaborate discussions on entropy stability of conservation laws and vanishing viscosity solutions see [21, 28]. Robust of numerical methods are often designed to mimic the estimate (9). However, numerical schemes can not satisfy the entropy inequality (8) and (9) for all convex entropy functions, but we want to show that it is satisfied for a specific entropy function. We will make the discussion more formal with the following definition.

Definition 2.1. Consider the nonlinear conservation law (1) subject to the smooth initial condition $\mathbf{u}(\mathbf{x}, 0) = \mathbf{u}_0(\mathbf{x})$. The system (1) is called entropy-stable if for all solutions $\mathbf{u} \in C^1(\Omega \times [0, T])$ we have $E(t) = E(0)$ and $E(t) \leq E(0)$ for all solutions $\mathbf{u} \notin C^1(\Omega \times [0, T])$, where $E(t)$ denotes the total entropy at $t \in [0, T]$.

As an initial example we will consider the inviscid Burgers' equation in 1D.

Example 2.1. The inviscid Burgers' equation is given by

$$\partial_t u + \partial_x f(u) = 0, \quad f(u) = \frac{1}{2}u^2 \quad x \in \Omega = [0, L], \quad (10)$$

subject to the initial condition $u(x, 0) = u_0(x)$ and periodic boundary conditions $u(0, t) = u(L, t)$ for all $t \geq 0$. Here the entropy pair is given by $e = \frac{1}{2}u^2$, $q = \frac{1}{3}u^3$ and the entropy variable is $\mathbf{g} = u$. Note that the Hessian is given by $H_u(e) = 1 > 0$, which is positive definite.

Entropy stability follows from standard energy method. That is, we consider

$$(\mathbf{g}, \partial_t u) + (\mathbf{g}, \partial_x f(u)) = (u, \partial_t u) + \left(u, \partial_x \left(\frac{1}{2}u^2 \right) \right) = 0. \quad (11)$$

The product rule gives the identity

$$\partial_x \left(\frac{1}{2}u^2 \right) = \frac{2}{3}\partial_x \left(\frac{u^2}{2} \right) + \frac{1}{3}u\partial_x u \equiv \frac{2}{3}\partial_x f(u) + \frac{1}{3}\partial_u f(u)\partial_x u. \quad (12)$$

Introducing the total entropy $E(t) = \int_{\Omega} e dx$ yielding

$$\partial_t E + \frac{1}{3}(u, \partial_x u^2) + \frac{1}{3}(u, u\partial_x u) = 0 \iff \partial_t E + \frac{1}{3}(u, \partial_x u^2) + \frac{1}{3}(u^2, \partial_x u) = 0. \quad (13)$$

Applying integration by parts, the volume terms cancel out, we find that

$$\partial_t E + \underbrace{\oint q \cdot n_x dx}_{q(L,t) - q(0,t)} = 0, \quad q = \frac{u^3}{3},$$

where n_x is the x -component of the unit outward normal. Finally, the boundary terms cancel out because of periodic boundary conditions, and we have

$$\partial_t E = 0.$$

Thus for smooth solutions total entropy E is conserved. When solution is discontinuous, we enforce the entropy inequality

$$\partial_t E \leq 0.$$

The next example is the 1D nonlinear shallow water equation in flux form.

Example 2.2. We consider the flux form of the nonlinear shallow water equations, which is given by

$$\partial_t h + \partial_x(hu) = 0, \quad (14a)$$

$$\partial_t(hu) + \partial_x\left(hu^2 + \frac{1}{2}gh^2\right) = 0. \quad (14b)$$

Here the conserved (prognostic) variables are the water height h and momentum hu . Thus, with $\mathbf{u} = [h, hu]^\top$

$$\partial_t \mathbf{u} + \partial_x \mathbf{f}(\mathbf{u}) = 0, \quad \mathbf{f}(\mathbf{u}) = \begin{bmatrix} hu \\ hu^2 + \frac{1}{2}gh^2 \end{bmatrix}. \quad (15)$$

Its elemental entropy function is given by the sum of the kinetic energy and potential energy densities,

$$e = \frac{1}{2} \frac{(hu)^2}{h} + \frac{1}{2} gh^2 = \frac{1}{2} hu^2 + \frac{1}{2} gh^2. \quad (16)$$

The entropy flux and entropy variables are given by

$$\mathbf{q} = \frac{1}{2} hu^3 + guh^2, \quad \mathbf{g} = \begin{bmatrix} gh - \frac{1}{2}u^2 \\ u \end{bmatrix}, \quad \mathbf{H}_\mathbf{u} = \begin{bmatrix} \frac{u^2+hg}{h} & -\frac{u}{h} \\ -\frac{u}{h} & \frac{1}{h} \end{bmatrix}.$$

For $h > 0$ the eigenvalues of the Hessian H_u are positive

$$\lambda_{\pm}(H_u) = \frac{u^2 + hg + 1}{h} \pm \sqrt{\left(\frac{u^2 + hg + 1}{h}\right)^2 - 4\frac{g}{h}} > 0. \quad (17)$$

Thus the Hessian is symmetric and positive definite for all flow regimes.

Using similar steps as above, we can show that the 1D shallow water equations (14) conserve the total entropy E . We consider

$$\begin{aligned} (\mathbf{g}, \partial_t \mathbf{u}) + (\mathbf{g}, \partial_x \mathbf{f}(\mathbf{u})) &= \left(gh - \frac{1}{2}u^2, \partial_t h\right) + (u, \partial_t(hu)) \\ &+ \left(gh - \frac{1}{2}u^2, \partial_x(hu)\right) + \left(u, \partial_x\left(hu^2 + \frac{1}{2}gh^2\right)\right) = 0. \end{aligned} \quad (18)$$

The product rule and the chain rule give the identity

$$\partial_x\left(hu^2 + \frac{1}{2}gh^2\right) = \frac{1}{2}(\partial_x(hu^2) + u\partial_x(hu) + (uh)\partial_x u) + (gh)\partial_x h. \quad (19)$$

Introducing (19) in (18), defining the total entropy $E(t) = \int_{\Omega} e dx$ and simplifying further yielding

$$\partial_t E + (gh, \partial_x(hu)) + (uh, \partial_x(gh)) + \frac{1}{2}(u, \partial_x(hu^2)) + \frac{1}{2}(hu^2, \partial_x u) = 0. \quad (20)$$

Using integration-by-parts we have

$$\partial_t E + \oint \mathbf{q} \cdot \mathbf{n}_x dx = 0, \quad \mathbf{q} = \frac{1}{2} hu^3 + guh^2.$$

Thus we have shown that the flux-form shallow water equations conserve energy.

Our final example is the 1D nonlinear shallow water equations in vector invariant form.

Example 2.3. Let us now consider the vector invariant form of the nonlinear shallow water equations, which is given by

$$\frac{\partial h}{\partial t} + \partial_x(hu) = 0, \quad (21a)$$

$$\frac{\partial u}{\partial t} + \partial_x\left(\frac{1}{2}u^2 + gh\right) = 0. \quad (21b)$$

The vector invariant form is well-suited for simulating subcritical flows, with $gh > u^2$, which are commonly observed in atmospheric and geostrophic flow problems [35, 54, 34, 19, 43]. Here, the prognostic variables are the water height h and flow velocity u . Thus, with $\mathbf{u} = [h, u]^\top$ we have

$$\partial_t \mathbf{u} + \partial_x \mathbf{f}(\mathbf{u}) = 0, \quad \mathbf{f}(\mathbf{u}) = \begin{bmatrix} hu \\ \frac{1}{2}u^2 + gh \end{bmatrix}. \quad (22)$$

The elemental entropy function is given by (16), that is

$$e = \frac{1}{2} \frac{(hu)^2}{h} + \frac{1}{2} gh^2 = \frac{1}{2} hu^2 + \frac{1}{2} gh^2.$$

The entropy variables and the Hessian are given by

$$\mathbf{g} = \left(gh + \frac{1}{2}u^2, hu \right)^\top, \quad H_u = \begin{bmatrix} g & u \\ u & h \end{bmatrix}. \quad (23)$$

When $h > 0$ and $gh > u^2$ the eigenvalues of the Hessian H_u given in (23) are positive

$$\lambda_{\pm}(H_u) = h + g \pm \sqrt{(h + g)^2 - 4(gh - u^2)} > 0.$$

Thus the Hessian is symmetric and positive definite for sub-critical flows, with $gh > u^2$ and $h > 0$.

Using the energy method, we can also prove that the vector invariant form of shallow water equations conserves total entropy/energy E . We consider

$$(\mathbf{g}, \partial_t \mathbf{u}) + (\mathbf{g}, \partial_x \mathbf{f}(\mathbf{u})) = \left(gh + \frac{1}{2}u^2, \partial_t h \right) + (uh, \partial_t h) \quad (24)$$

$$+ \left(gh + \frac{1}{2}u^2, \partial_x (hu) \right) + \left(uh, \partial_x \left(gh + \frac{1}{2}u^2 \right) \right) = 0. \quad (25)$$

Using integration-by-parts, we have

$$\partial_t E + \oint \mathbf{q} \cdot \mathbf{n}_x dx = 0, \quad \mathbf{q} = \frac{1}{2} hu^3 + guh^2.$$

Thus the vector invariant form of shallow water equations conserve total entropy/energy.

This strategy of showing that some total energy/entropy-like quantity is non-increasing, that is $\partial_t E \leq 0$, is called the energy method. Note that for the vector invariant form of the nonlinear shallow water equations (21), the only tool needed to prove entropy/energy stability is integration by parts. However, the Burger's equation (10) and the flux form of the nonlinear shallow water equations (14) require both the product rule and the chain rule, as well as integration by parts. This is generally true for many important nonlinear conservation laws, such as the Euler equations of compressible gas dynamics. While discrete numerical derivative and integration operators can be designed to emulate integration by parts, it is challenging (or impossible) to design numerical operators to mimic the chain rule or product rule at the discrete level for general functions. To enable the development of robust and provably entropy/energy stable numerical schemes, equations at the continuous level must be rewritten into the so-called skew-symmetric form so that we can forgo the use of chain/product rule when performing the energy method.

2.3 Skew-symmetric splitting

For several nonlinear conservation laws the energy method requires the use of the chain rule or product rule, which discrete differential operators usually do not mimic. Fortunately, one can manipulate a set of continuous equations into a mathematically equivalent form known as the skew-symmetric form, for which the energy method can be applied without the use of chain rule or product rule. Then for the semi-discretisation of the skew-symmetric form one can make a semi-discrete energy method argument without the need for the discrete spatial derivative to obey the product/chain rule. As long as a skew-symmetric form exists for a given PDE, one can show semi-discrete energy stability via the use of SBP operators which we will introduce in Section 4.

Typically, a skew-symmetric form is found by applying divergence flux splitting, which is really a convex combination of the flux form (1) and the quasi-linear form (3). For a scalar PDE flux $f(u)$ we have

$$\partial_x f(u) = (1 - \alpha) \partial_x f + \alpha \partial_u f \partial_x u, \quad 0 \leq \alpha \leq 1. \quad (26)$$

Example 2.4. For example, $\alpha = 1/3$ gives the skew-symmetric form of the Burger's equation

$$\partial_t u + \frac{2}{3} \partial_x \frac{u^2}{2} + \frac{1}{3} u \partial_x u = 0. \quad (27)$$

As before we multiply (27) by $\mathbf{g} = u$ and integrate over the domain,

$$(u, \partial_t u) + \frac{1}{3} (u, \partial_x u^2) + \frac{1}{3} (u, u \partial_x u) = 0. \quad (28)$$

We integrate by parts and we have

$$\partial_t E + \oint \mathbf{q} \cdot \mathbf{n}_x dx = 0, \quad \mathbf{q} = \frac{u^3}{3}.$$

Example 2.5. The skew-symmetric form of the nonlinear shallow water equation in flux form is

$$\frac{\partial h}{\partial t} + \partial_x (hu) = 0 \quad (29a)$$

$$\frac{\partial (hu)}{\partial t} + \frac{1}{2} \partial_x (hu^2) + \frac{1}{2} u \partial_x (hu) + \frac{1}{2} hu \partial_x u + gh \partial_x h = 0. \quad (29b)$$

Again we multiply (29) by $\mathbf{g}^\top = [gh - \frac{1}{2}u^2, u]$, integrating over the domain and simplifying further yielding

$$\partial_t E + (gh, \partial_x (hu)) + (uh, \partial_x (gh)) + \frac{1}{2} (u, \partial_x (hu^2)) + \frac{1}{2} (hu^2, \partial_x (u)) = 0. \quad (30)$$

Using integration-by-parts having

$$\partial_t E + \oint \mathbf{q} \cdot \mathbf{n}_x dx = 0, \quad \mathbf{q} = \frac{1}{2} hu^3 + guh^2.$$

We will try to make the discussion more general so that it is applicable to the multi-dimensional model problem (1). Let us consider the skew-symmetric equivalent form of (1)

$$\partial_t \mathbf{u} + \mathbf{F}(\mathbf{u}, \mathbf{f}(\mathbf{u}), \partial_{\mathbf{x}}) = 0, \quad \mathbf{F}(\mathbf{u}, \mathbf{f}(\mathbf{u}), \partial_{\mathbf{x}}) \equiv \nabla \cdot \mathbf{f}(\mathbf{u}), \quad \mathbf{x} \in \Omega \subset \mathbb{R}^d, \quad t \geq 0. \quad (31)$$

Here $\mathbf{F}(\mathbf{u}, \mathbf{f}(\mathbf{u}), \partial_{\mathbf{x}})$ is a functional equivalence of the divergence of the flux $\nabla \cdot \mathbf{f}(\mathbf{u})$ obtained by taken a linear combination of the conservative terms and non-conservative products, as above, such that

$$(\mathbf{g}, \mathbf{F}(\mathbf{u}, \mathbf{f}(\mathbf{u}), \partial_{\mathbf{x}})) = (1, \nabla \cdot \mathbf{q}) = \oint_{\partial\Omega} (\mathbf{q} \cdot \mathbf{n}) d\mathbf{x}, \quad (32)$$

holds by only applying integration-by-parts, and without the chain/product rule.

More importantly, we can prove entropy conservation using only integration-by-parts, and without the chain/product rule. That is

$$\underbrace{(\mathbf{g}, \partial_t \mathbf{u})}_{\frac{d}{dt} E(t) = \frac{d}{dt} (1, e)} + \underbrace{(\mathbf{g}, \mathbf{F}(\mathbf{u}, \mathbf{f}(\mathbf{u}), \partial_{\mathbf{x}}))}_{(1, \nabla \cdot \mathbf{q})} = 0 \implies \frac{d}{dt} E(t) = - \oint_{\partial\Omega} (\mathbf{q} \cdot \mathbf{n}) d\mathbf{x} = 0. \quad (33)$$

Other than the primary motivation of showing entropy stability using only integration by parts, it is also desirable that the skew-symmetric form ensure that the proof of the conservative property (2) uses only integration by parts without the chain rule. That is

$$\underbrace{(1, \mathbf{F}_i(\mathbf{u}, \mathbf{f}(\mathbf{u}), \partial_{\mathbf{x}}))}_{(1, \nabla \cdot \mathbf{f}_i)} = \oint_{\partial\Omega} (\mathbf{f}_i(\mathbf{u}) \cdot \mathbf{n}) d\mathbf{x}, \quad \forall i = 1, 2, \dots, m, \quad (34)$$

thus implying

$$\partial_t \mathcal{U}_i = (1, \partial_t \mathbf{u}_i) = - \underbrace{(1, \mathbf{F}_i(\mathbf{u}, \mathbf{f}_i(\mathbf{u}), \partial_{\mathbf{x}}))}_{(1, \nabla \cdot \mathbf{f}_i)} = - \oint_{\partial\Omega} (\mathbf{f}_i(\mathbf{u}) \cdot \mathbf{n}) d\mathbf{x}. \quad (35)$$

As noted earlier, for nonlinear hyperbolic conservation laws with weak solutions, the conservative properties of a numerical method is critical for the convergence of numerical solutions [3]. For the Burger's equation with $f(u) = u^2/2$, from (27), we have

$$F(u, f(u), \partial_x) = \frac{2}{3} \partial_x f(u) + \frac{1}{3} \partial_u f \partial_x u \equiv \frac{2}{3} \partial_x \frac{u^2}{2} + \frac{1}{3} u \partial_x u.$$

Using only integration by parts we also have

$$\begin{aligned} (1, F(u, f(u), \partial_x)) &= \frac{1}{3} (1, \partial_x u^2) + \frac{1}{3} (1, u \partial_x u) \\ &= \frac{1}{6} (\partial_x u, u) - \frac{1}{6} (u, \partial_x u) + \frac{1}{2} \oint_{\partial\Omega} u^2 dx = \frac{1}{2} \oint_{\partial\Omega} u^2 dx, \end{aligned}$$

and having

$$\partial_t \mathcal{U} = (1, \partial_t u) = -\frac{1}{2} \oint_{\partial\Omega} u^2 dx. \quad (36)$$

For the nonlinear shallow water equation in flux form, with

$$\mathbf{f}(\mathbf{u}) = \begin{bmatrix} hu \\ hu^2 + \frac{1}{2}gh^2 \end{bmatrix},$$

from (29) we have

$$\mathbf{F}(\mathbf{u}, \mathbf{f}(\mathbf{u}), \partial_x) = \begin{bmatrix} \frac{1}{2} \partial_x (hu^2) + \frac{1}{2} u \partial_x (hu) + \frac{1}{2} hu \partial_x u + gh \partial_x h \end{bmatrix}. \quad (37)$$

Similarly using only integration by parts we also have

$$\begin{aligned} \int_{\Omega} \mathbf{F}(\mathbf{u}, \mathbf{f}(\mathbf{u}), \partial_x) dx &= \begin{bmatrix} \frac{1}{2} (1, \partial_x (hu^2)) + \frac{1}{2} (1, u \partial_x (hu)) + \frac{1}{2} (1, hu \partial_x u) + \frac{1}{2} (1, gh \partial_x h) \end{bmatrix} \\ &= \begin{bmatrix} \oint_{\partial\Omega} ((hu) \cdot n_x) dx \\ \frac{g}{4} (\partial_x h, h) - \frac{g}{4} (h, \partial_x h) + \oint_{\partial\Omega} ((hu^2 + \frac{1}{2}gh^2) \cdot n_x) dx \end{bmatrix} \\ &= \begin{bmatrix} \oint_{\partial\Omega} ((hu) \cdot n_x) dx \\ \oint_{\partial\Omega} ((hu^2 + \frac{1}{2}gh^2) \cdot n_x) dx \end{bmatrix} = \oint_{\partial\Omega} (\mathbf{f}(\mathbf{u}) \cdot \mathbf{n}_x) dx, \end{aligned}$$

and

$$\partial_t \mathcal{U} = - \int_{\Omega} \mathbf{F}(\mathbf{u}, \mathbf{f}(\mathbf{u}), \partial_x) dx = - \oint_{\partial\Omega} (\mathbf{f}(\mathbf{u}) \cdot \mathbf{n}_x) dx. \quad (38)$$

To complete the discussion we give a 2D example. We consider the 2D shallow water equations in flux form, with

$$\mathbf{u} = [h, hu, hv]^T, \quad \mathbf{f}(\mathbf{u}) = [\mathbf{f}_x, \mathbf{f}_y], \quad \mathbf{f}_x = \begin{bmatrix} hu \\ hu^2 + \frac{1}{2}gh^2 \\ huv \end{bmatrix}, \quad \mathbf{f}_y = \begin{bmatrix} hv \\ huv \\ hv^2 + \frac{1}{2}gh^2 \end{bmatrix}, \quad (39)$$

where $\mathbf{v} = [u, v]^T$ is the fluid velocity vector, h is the height of the fluid, and g is the gravitational acceleration. The skew symmetric form is given by (31) with $\partial_x = (\partial_x, \partial_y)$ and

$$\mathbf{F}(\mathbf{u}, \mathbf{f}(\mathbf{u}), \partial_x) = \begin{bmatrix} \partial_x(hu) + \partial_y(hv) \\ \frac{1}{2} (\partial_x(hu^2) + u \partial_x(hu) + (hu) \partial_x u) + gh \partial_x h + \frac{1}{2} (\partial_y(huv) + u \partial_y(hv) + (hv) \partial_y u) \\ \frac{1}{2} (\partial_y(hv^2) + v \partial_y(hv) + (hv) \partial_y v) + gh \partial_y h + \frac{1}{2} (\partial_x(huv) + u \partial_x(hv) + (hv) \partial_x u) \end{bmatrix}. \quad (40)$$

The entropy function, flux and variables $(e, \mathbf{q}, \mathbf{g})$ are given by

$$e = \frac{1}{2} h(u^2 + v^2) + \frac{1}{2} gh^2, \quad \mathbf{q} = \begin{bmatrix} \left(\frac{1}{2} hu(u^2 + v^2) + guh^2 \right) \\ \left(\frac{1}{2} hv(u^2 + v^2) + ghv^2 \right) \end{bmatrix}, \quad \mathbf{g} = \begin{bmatrix} gh - \frac{1}{2}(u^2 + v^2) \\ u \\ v \end{bmatrix}. \quad (41)$$

As above, it is possible to show that (32) as well as (34)–(35) hold using only integration-by-parts, without the chain or product rule. In the appendix we give more examples of the skew-symmetric forms for the 1D and 2D Euler equations of gas dynamics.

3 The SBP finite difference framework for d/dx

In order to construct provably entropy-stable and conservative numerical methods for nonlinear conservation laws, we will mimic the entropy-stability and conservative properties of the continuous problem. To replicate the continuous analysis at the discrete level our discrete differential operators must satisfy the integration by parts principle. To be specific, for $f, g \in C^1(\Omega)$, where $\Omega = [0, L]$ is the spatial domain, we introduce the integration by parts property for the first derivative operator d/dx

$$\left(\frac{df}{dx}, g\right) + \left(f, \frac{dg}{dx}\right) = B(fg) := \oint (fg) \cdot n_x dx = fg|_{x=L} - fg|_{x=0}, \quad (42)$$

where n_x is the x -component of the normal vector on the boundary, that is $n_x = -1$ at $x = 0$ and $n_x = 1$ at $x = L$. As Discrete approximations of the first derivative operator d/dx that satisfy the integration by parts property (42) are called SBP operators [39, 51, 38]. We will give the formal definitions below. First we will discuss the traditional SBP framework [39, 38], formulated through the assumptions given [48]. We will end the section by presenting the recent DP SBP framework of [48, 47].

For $N \in \mathbb{N}$ we define the uniformly spaced grid points given by

$$x_j = (j-1)\Delta x, \quad \Delta x = \frac{L}{N-1}, \quad L > 0, \quad j \in \{1, 2, 3, \dots, N\}. \quad (43)$$

Given $f \in L^2([0, L])$ we denote the grid function by \mathbf{f} , that is the restriction of f on the grid, by

$$\mathbf{f} := (f(x_1), \dots, f(x_N))^T \in \mathbb{R}^N. \quad (44)$$

We introduce the positive definite diagonal matrix

$$H := \text{diag}((h_1, \dots, h_N)) \in \mathbb{R}^{N \times N}, \quad h_j > 0, \quad j \in \{1, \dots, N\}, \quad (45)$$

and the discrete inner-product

$$\langle \mathbf{f}, \mathbf{g} \rangle_H := \mathbf{f}^T H \mathbf{g} = \sum_{j=1}^N h_j f(x_j) g(x_j). \quad (46)$$

We note that $h_j = \Delta x w_j > 0$ with the constants $w_j > 0$ being the weights of a composite quadrature rule and $\Delta x > 0$ is the spatial step. In this way, for a grid function \mathbf{g} the multiplication by $\mathbb{1}^T H$ with $\mathbb{1} = (1, \dots, 1)^T \in \mathbb{R}^N$, from the left, may be interpreted as a numerical quadrature given

$$\langle \mathbb{1}, \mathbf{g} \rangle_H = \mathbb{1}^T H \mathbf{g} = \sum_{j=1}^N h_j g(x_j) \approx \int_0^L g(x) dx. \quad (47)$$

3.1 Traditional SBP finite difference operators

As given in [48], the traditional SBP framework [39, 38] for the first derivative d/dx , with a diagonal norm, can be expressed through the following assumptions:

(A.1) There exists $H : \mathbb{R}^N \rightarrow \mathbb{R}^N$ which defines a positive discrete measure

$$\langle \mathbf{g}, \mathbf{g} \rangle_H = \mathbf{g}^T H \mathbf{g} > 0, \quad \forall \mathbf{g} \in \mathbb{R}^N, \quad (48)$$

$$\langle \mathbb{1}, \mathbf{g} \rangle_H = \mathbb{1}^T H \mathbf{g} = \sum_{j=1}^N h_j g(x_j) \rightarrow \int_0^L g(x) dx, \quad (49)$$

and for $g \in L^2([0, L])$ converges weakly as $n \rightarrow \infty$.

(A.2) There exists $D : \mathbb{R}^N \rightarrow \mathbb{R}^N$ with

$$(D\mathbf{f})_j = \left. \frac{df(x)}{dx} \right|_{x_j}, \quad \forall j \in \{1, 2, \dots, N\},$$

for all $f \in V^p$ where V^p is a polynomial space of at most degree $p \geq 0$.

(A.3) The linear operator $D : \mathbb{R}^N \rightarrow \mathbb{R}^N$ obeys

$$\langle D\mathbf{f}, \mathbf{g} \rangle_H + \langle \mathbf{f}, D\mathbf{g} \rangle_H = B(fg) := f_N g_N - f_1 g_1, \quad (50)$$

for all $\mathbf{f}, \mathbf{g} \in \mathbb{R}^N$.

Assumption (A.1) equips the solution space with a numerical quadrature rule and a discrete l_2 -norm defined by

$$\|\mathbf{g}\|_H^2 := \langle \mathbf{g}, \mathbf{g} \rangle_H > 0, \quad \forall \mathbf{g} \in \mathbb{R}^N.$$

Assumption (A.2) encodes a consistent discrete first derivative operator $D : \mathbb{R}^N \rightarrow \mathbb{R}^N$ such that for a smooth function u , with $\mathbf{u} \in \mathbb{R}^N$ and $u_j = u(x_j)$, we have

$$(D\mathbf{u})_j = \frac{du}{dx} \Big|_{x=x_j} + \mathbb{T}_j, \quad \mathbb{T}_j = O(\Delta x^p), \quad \forall j \in \{1, 2, \dots, N\},$$

where \mathbb{T}_j are the truncation errors on the grid. For finite difference SBP operators the accuracy of the derivative operator is not uniform for all grid points x_j . We can thus write the truncation error of an SBP operator as

$$\mathbb{T}_j = \begin{cases} \Delta x^\gamma \beta_j \frac{\partial^{\gamma+1} u}{\partial x^{\gamma+1}} \Big|_{x=x_j}, & 1 \leq j \leq s \text{ or } (N-s+1) \leq j \leq n, \\ \Delta x^\nu \beta_j \frac{\partial^{\nu+1} u}{\partial x^{\nu+1}} \Big|_{x=x_j}, & s+1 \leq j \leq (N-s), \end{cases} \quad (51)$$

Here $s \geq 1$, β_j are mesh independent constants, $\gamma \geq 1$ is the accuracy of the boundary stencils and $\nu > \gamma$ is the accuracy of the interior stencils. In particular for traditional SBP operators we have $\gamma = p$ and $\nu = 2p$, where $p = 1, 2, \dots$.

Assumption (A.3) is the SBP property and equips $D : \mathbb{R}^N \rightarrow \mathbb{R}^N$ with the integration by parts principle (42) which will be critical for proving numerical (entropy-)stability. Assumption (A.3) can also be rewritten in matrix form. Note that for $B : \mathbb{R}^N \rightarrow \mathbb{R}^N$ we have

$$\mathbf{f}(HD + (HD)^T)\mathbf{g} = f_N g_N - f_1 g_1 = \mathbf{f}^T B \mathbf{g}, \quad B := \mathbf{e}_N \mathbf{e}_N^T - \mathbf{e}_1 \mathbf{e}_1^T = \begin{bmatrix} -1 & & & \\ & 0 & & \\ & & \ddots & \\ & & & 0 \\ & & & & 1 \end{bmatrix}, \quad (52)$$

where $\mathbf{e}_1 = (1, 0, \dots, 0)^T \in \mathbb{R}^N$, $\mathbf{e}_N = (0, 0, \dots, 1)^T \in \mathbb{R}^N$ are the 1-st and N -th unit vectors in \mathbb{R}^N , and having

$$Q = HD, \quad Q + Q^T = B, \quad H = H^T > 0. \quad (53)$$

In the literature [39, 38], the relation (53) often defines the SBP property.

Traditional SBP operators are centered finite difference stencils closed at the boundaries with one-sided finite difference stencils such that Assumptions (A.1)–(A.3) hold. An example of a traditional SBP operator is the 2-tuple (D, H) given by

$$D = \frac{1}{\Delta x} \begin{bmatrix} -1 & 1 & & & \\ -\frac{1}{2} & 0 & \frac{1}{2} & & \\ & -\frac{1}{2} & 0 & \frac{1}{2} & \\ & & \ddots & \ddots & \ddots \\ & & & -\frac{1}{2} & 0 & \frac{1}{2} \\ & & & & -1 & 1 \end{bmatrix}, \quad H = \Delta x \begin{bmatrix} \frac{1}{2} & & & & \\ & 1 & & & \\ & & \ddots & & \\ & & & 1 & \\ & & & & \frac{1}{2} \end{bmatrix}, \quad (54)$$

with boundary accuracy $\gamma = 1$ and interior accuracy $\nu = 2$.

3.2 DP upwind SBP finite difference operators

Recently DP SBP framework [47, 46, 48] was introduced to improve accuracy and flexibility of numerical approximations. The DP SBP operators are a pair of forward and backward finite difference stencils that together obey the SBP property. As shown in [48], the DP upwind SBP framework for the first derivative d/dx [47, 46] can be expressed through the following assumptions:

(B.1) There exists $H : \mathbb{R}^N \rightarrow \mathbb{R}^N$ which defines a positive discrete measure

$$\langle \mathbf{g}, \mathbf{g} \rangle_H = \mathbf{g}^T H \mathbf{g} > 0, \quad \forall \mathbf{g} \in \mathbb{R}^N, \quad (55)$$

$$\langle \mathbb{1}, \mathbf{g} \rangle_H = \mathbb{1}^T H \mathbf{g} = \sum_{j=1}^N h_j g(x_j) \rightarrow \int_0^L g(x) dx, \quad (56)$$

and for $g \in L^2([0, L])$ converges weakly as $n \rightarrow \infty$.

(B.2) There exists a pair of linear operators $D_{\pm} : \mathbb{R}^N \rightarrow \mathbb{R}^N$ with

$$(D_{\pm} \mathbf{f})_j = \left. \frac{df(x)}{dx} \right|_{x=x_j}, \quad \forall j \in \{1, 2, \dots, N\},$$

for all $f \in V^p$ where V^p is a polynomial space of at most degree $p \geq 0$.

(B.3) The linear operators $D_{\pm} : \mathbb{R}^N \rightarrow \mathbb{R}^N$ together obey

$$\langle D_+ \mathbf{f}, \mathbf{g} \rangle_H + \langle \mathbf{f}, D_- \mathbf{g} \rangle_H = B(fg) := f_N g_N - f_1 g_1, \quad (57)$$

for all $\mathbf{f}, \mathbf{g} \in \mathbb{R}^N$.

(B.4) The linear operators $D_{\pm} : \mathbb{R}^N \rightarrow \mathbb{R}^N$ together obey

$$\langle \mathbf{f}, (D_+ - D_-) \mathbf{f} \rangle_H \leq 0, \quad (58)$$

for all $\mathbf{f} \in \mathbb{R}^N$.

As before, Assumption (B.1) equips the solution space with a numerical quadrature rule and a discrete l_2 -norm defined by

$$\|\mathbf{g}\|_H^2 := \langle \mathbf{g}, \mathbf{g} \rangle_H > 0, \quad \forall \mathbf{g} \in \mathbb{R}^N.$$

Similarly, Assumption (B.2) encodes a consistent discrete first derivative operator $D_{\pm} : \mathbb{R}^N \rightarrow \mathbb{R}^N$ such that for a smooth function u , with $\mathbf{u} \in \mathbb{R}^N$ and $u_j = u(x_j)$, we have

$$(D_{\pm} \mathbf{u})_j = \left. \frac{du}{dx} \right|_{x=x_j} + \mathbb{T}_j^{\pm}, \quad \mathbb{T}_j^{\pm} = O(\Delta x^p), \quad \forall j \in \{1, 2, \dots, N\}. \quad (59)$$

Assumption (B.3) is the DP SBP property which is equivalent

$$Q_{\pm} = H D_{\pm}, \quad Q_- + Q_+^T = B, \quad H = H^T > 0, \quad (60)$$

where B define in (52). In particular, Assumption (B.3) equips $D_{\pm} : \mathbb{R}^N \rightarrow \mathbb{R}^N$ with the integration by parts principle, which is critical for proving numerical stability.

Assumption (B.4) is the upwind DP property, which is equivalent to

$$A = H(D_+ - D_-), \quad A = A^T, \quad \mathbf{g}^T A \mathbf{g} \leq 0, \quad \forall \mathbf{g} \in \mathbb{R}^N. \quad (61)$$

An example of a DP SBP operator is the 3-tuple (D_-, D_+, H) given by

$$D_- = \frac{1}{\Delta x} \begin{bmatrix} -1 & 1 & & & & & \\ -1 & 1 & & & & & \\ \frac{1}{2} & -2 & \frac{3}{2} & & & & \\ & \frac{1}{2} & -2 & \frac{3}{2} & & & \\ & & \ddots & \ddots & \ddots & & \\ & & & \frac{1}{2} & -2 & \frac{3}{2} & \\ & & & & \frac{1}{2} & -2 & \frac{3}{2} \\ & & & & & \frac{1}{2} & -2 & \frac{3}{2} \\ & & & & & & \frac{1}{2} & -2 & \frac{3}{2} \end{bmatrix}, \quad D_+ = \frac{1}{\Delta x} \begin{bmatrix} -3 & 5 & -2 & & & & \\ -\frac{1}{5} & -1 & \frac{8}{5} & -\frac{2}{5} & & & \\ & -\frac{3}{2} & 2 & -\frac{1}{2} & & & \\ & & -\frac{3}{2} & 2 & -\frac{1}{2} & & \\ & & & \ddots & \ddots & \ddots & \\ & & & & -\frac{3}{2} & 2 & -\frac{1}{2} \\ & & & & & -1 & 1 & -\frac{1}{2} \\ & & & & & & -1 & 1 \end{bmatrix}, \quad (62)$$

$$H = \Delta x \begin{bmatrix} \frac{1}{4} & & & & & & \\ & \frac{5}{4} & & & & & \\ & & 1 & & & & \\ & & & \ddots & & & \\ & & & & 1 & & \\ & & & & & \frac{5}{4} & \\ & & & & & & \frac{1}{4} \end{bmatrix},$$

with boundary accuracy $\gamma = 1$ and interior accuracy $\nu = 2$.

Close to the boundaries, the SBP operators [47, 39, 48] considered in this study are closed with lower order accurate stencils of $\gamma = (\nu/2)$ -th for even ν , and $\gamma = (\nu - 1)/2$ -th order of accuracy for odd ν , where $\nu \geq 1$ is accuracy of the interior stencil. The global convergence rate of stable SBP finite difference schemes is limited by the accuracy of the boundary stencils. As it is well-known [55, 56, 57], for first order systems, convergent SBP schemes with ν -th order accurate interior stencils and γ -th order accurate boundary stencils, where $\gamma < \nu$, will yield $(\gamma + 1)$ -th order global convergence rate. We summarise the discussions in Table 1 below.

Interior	1	2	3	4	5	6	7	8	9
Boundary	0	1	1	2	2	3	3	4	4
Global	1	2	2	3	3	4	4	5	5

Table 1: Expected accuracy of SBP operators for first order systems.

As discussed in [48], a main benefit of the DP-SBP framework [47, 48] over traditional SBP schemes [39] is there are a pair of derivative operators and more degree of freedom, which enable the flexibility and possibility of designing numerical schemes with special qualities which could potentially capture important characteristics of a target application. For example, for conservative PDE systems, we can design energy conserving schemes, thanks to the DP-SBP property Assumption (B.3), and the fact that if

$$\mathcal{Q}_{\pm} := Q_{\pm} - \frac{1}{2}B, \quad \mathcal{Q}_{\pm} := HD_{\pm} \quad (63)$$

then $\mathcal{Q}_{-} + \mathcal{Q}_{+}^T = 0$. We can also construct energy dissipating schemes, for example to upwind transport terms in our systems or dissipate unresolved modes for nonlinear problems. This is mainly a consequence of upwind DP-SBP, Assumption (B.4). In the current work we will focus on entropy dissipating schemes for robust and accurate simulations of nonlinear hyperbolic conservation laws.

Remark 1. The traditional SBP operator (D, H) also satisfies DP-SBP framework, that is Assumptions (B.1)–(B.4), with $D_{-} = D_{+} = D$ and $(\mathbf{f}, (D_{+} - D_{-})\mathbf{f})_H = 0$. Similarly, given the upwind DP-SBP operator (D_{-}, D_{+}, H) which satisfies Assumptions (B.1)–(B.4), the averaged operator $D := \frac{1}{2}(D_{+} + D_{-})$ is a centred difference based SBP operator which satisfies the traditional SBP framework, that is Assumptions (A.1)–(A.3).

Remark 2. Despite being a finite-difference scheme, the SBP operators are, in essence, approximations of weak derivatives, where the test space of functions is V^p , [48]. This creates a numerical structure parallel to the theoretical underpinnings of both finite elements and discontinuous Galerkin schemes, as used for the weak formulation of a given problem.

4 Semi-discrete approximation

We will now discuss how to derive conservative, robust and provably entropy stable semi-discrete approximations of nonlinear hyperbolic conservation laws using upwind DP-SBP finite difference operators. To simplify the presentation, we will consider systems of conservation laws in 1D. However, the ideas and discussions easily generalize to systems of nonlinear conservation laws in higher space dimensions, 2D and 3D.

To begin, we consider the 1D hyperbolic conservation law

$$\partial_t u + \partial_x \mathbf{f}(\mathbf{u}) = 0, \quad x \in \Omega = [0, L], \quad t \geq 0, \quad (64)$$

where $\mathbf{f}(\mathbf{u})$ is the flux function, $L > 0$ is the length of the spatial interval $\Omega \subset \mathbb{R}$. We close the boundaries at $x = \{0, L\}$ with periodic boundary conditions, that is

$$\mathbf{u}(0, t) = \mathbf{u}(L, t) \quad \text{and} \quad \mathbf{f}(\mathbf{u}(0, t)) = \mathbf{f}(\mathbf{u}(L, t)). \quad (65)$$

Thus for smooth solutions, the system (64) with (65) satisfies (35) and (33), that is

$$\partial_t \mathcal{U} = \mathbf{f}(\mathbf{u}(0, t)) - \mathbf{f}(\mathbf{u}(L, t)) = 0, \quad (66)$$

$$\frac{d}{dt} E(t) = q(\mathbf{u}(0, t)) - q(\mathbf{u}(L, t)) = 0. \quad (67)$$

To be useful, numerical approximations of (64) with periodic boundary conditions (65) must as far as possible mimic (66) and (67) at the discrete level, leading to conservative and entropy-stable discrete approximations.

4.1 Finite volume flux splitting and linear stability

To enable the effectiveness of the upwind features of the DP SBP operators we will need a splitting strategy. We will consider classical flux splitting which is prevalent in the finite volume literature, see for examples [21, 4, 22, 50, 49]. Next we introduce the upwind flux splitting where

$$\mathbf{f}_i(\mathbf{u}) = \underbrace{\frac{1}{2}(\mathbf{f}_i + \gamma_i \mathbf{g}_i)}_{\mathbf{f}_i^+} + \underbrace{\frac{1}{2}(\mathbf{f}_i - \gamma_i \mathbf{g}_i)}_{\mathbf{f}_i^-} \equiv \mathbf{f}_i^+ + \mathbf{f}_i^-, \quad i = 1, 2, \dots, m, \quad (68)$$

$\gamma_i \geq 0$ are (time-dependent) constants and \mathbf{g}_i are carefully chosen functions to induce dissipation when upwinded. We will denote \mathbf{f}^+ the positive-going flux and \mathbf{f}^- is the negative-going flux. If $\mathbf{g}_i = \mathbf{u}_i$ and $\gamma_i = \max_x |\max_j \lambda_j(A_x)|$ where $A_x = \partial_{\mathbf{u}} \mathbf{f}$, then we get the classical global Lax-Friederich flux splitting [21, 22].

We discretise the spatial interval $\Omega = [0, L]$ using the uniform grid (43), and sample the solution and flux on the grid, having

$$\mathbf{u}_i(t) := (\mathbf{u}(x_1, t), \dots, \mathbf{u}(x_n, t))^T, \quad \mathbf{f}_i^\pm(\mathbf{u}) := (\mathbf{f}_i^\pm(\mathbf{u}(x_1, t)), \dots, \mathbf{f}_i^\pm(\mathbf{u}(x_N, t)))^T, \quad i = 1, 2, \dots, m. \quad (69)$$

To approximate the divergence of the flux we will use the dual-pairing operators to upwind the positive-going flux \mathbf{f}^+ and the negative-going flux \mathbf{f}^- having

$$\partial_x \mathbf{f}(\mathbf{u}) \approx (I_m \otimes D_+) \mathbf{f}^- + (I_m \otimes D_-) \mathbf{f}^+ = (I_m \otimes D) \mathbf{f} - \frac{1}{2} (\Gamma \otimes (D_+ - D_-)) \mathbf{g}, \quad (70)$$

where $D := \frac{1}{2} (D_+ + D_-)$, $\Gamma = \text{diag}([\gamma_1, \gamma_2, \dots, \gamma_m])$, $\gamma_i \geq 0$ for $i = 1, 2, \dots, m$, and \otimes denote the Kronecker product. Note that for smooth solutions we have $|\Gamma \otimes (D_+ - D_-) \mathbf{g}| = O(\Delta x^{2p-1})$ where $p \geq 1$ is the order of accuracy of the difference operators D_\pm .

The periodic boundary conditions $\mathbf{u}|_{x_1=0} = \mathbf{u}|_{x_N=L}$ and $\mathbf{f}(\mathbf{u})|_{x_1=0} = \mathbf{f}(\mathbf{u})|_{x_N=L}$ can be implemented using a penalty method [52]. In particular, we consider the penalized SBP operators

$$\tilde{D}_\pm = D_\pm + H^{-1} B_N, \quad B_N = \frac{1}{2} (\mathbf{e}_1 \mathbf{e}_1^T - \mathbf{e}_1 \mathbf{e}_N^T + \mathbf{e}_N \mathbf{e}_1^T - \mathbf{e}_N \mathbf{e}_N^T), \quad (71)$$

where $\mathbf{e}_1 = (1, 0, \dots, 0)^T \in \mathbb{R}^N$, $\mathbf{e}_N = (0, 0, \dots, 1)^T \in \mathbb{R}^N$ are the 1-st and N -th unit vectors in \mathbb{R}^N . Note that

$$B_N \mathbf{f} = \frac{1}{2} \begin{bmatrix} f_1 - f_N \\ 0 \\ \vdots \\ 0 \\ f_1 - f_N \end{bmatrix}, \quad \forall \mathbf{f} \in \mathbb{R}^N, \quad (72)$$

is a weak implementation of the periodic boundary condition $f(x_1) = f(x_N)$, and

$$\langle \tilde{D}_+ \mathbf{f}, \mathbf{g} \rangle_H + \langle \mathbf{f}, \tilde{D}_- \mathbf{g} \rangle_H = 0, \quad \langle \mathbf{f}, (\tilde{D}_+ - \tilde{D}_-) \mathbf{f} \rangle_H = \langle \mathbf{f}, (D_+ - D_-) \mathbf{f} \rangle_H \leq 0, \quad (73)$$

for all $\mathbf{f}, \mathbf{g} \in \mathbb{R}^N$.

For simplicity, we will ignore the \sim in the penalized SBP operators and write $\tilde{D}_\pm = D_\pm$ where D_\pm are periodic operators implemented using periodic penalties as in (71) or through injection by using periodic boundary stencils.

A semi-discrete approximation of the systems of 1D conservation laws (64) reads

$$\partial_t \mathbf{u} + (I_m \otimes D) \mathbf{f} = \frac{1}{2} (\Gamma \otimes (D_+ - D_-)) \mathbf{g}, \quad \Gamma = \text{diag}([\gamma_1, \gamma_2, \dots, \gamma_m]), \quad \gamma_i > 0, \quad (74)$$

where $D := \frac{1}{2} (D_+ + D_-)$, $\mathbf{f} \in \mathbb{R}^{mN}$ is the discrete PDE flux and $\mathbf{g} \in \mathbb{R}^{mN}$ is carefully chosen function to induce dissipation. For the semi-discrete approximation (74), the discrete conservative principle follows in a straightforward manner. We formulate the result as the theorem.

Theorem 4.1. Consider the semi-discrete upwind DP-SBP approximation (74) of the system (64) with periodic boundary conditions (65) implemented weakly through (71). If the 3-tuple (D_-, D_+, H) satisfies the upwind DP SBP operator given by Assumptions (B.1)–(B.4), then the semi-discrete total quantity $\mathcal{U}_{ih}(t) = \langle \mathbf{1}, \mathbf{u}_i \rangle_H$ satisfies

$$\frac{d}{dt} \mathcal{U}_{ih}(t) = \langle D \mathbf{1}, \mathbf{f}_i \rangle_H + \frac{\gamma_i}{2} \langle (D_+ - D_-) \mathbf{1}, \mathbf{g}_i \rangle_H = 0, \quad \forall i = 1, 2, \dots, m, \quad (75)$$

where $\gamma_i > 0$ and $A = H(D_+ - D_-) = A^\top \geq 0$ is a symmetric and negative semi-definite matrix.

Proof. For all $i = 1, 2, \dots, m$, we consider

$$\underbrace{\langle \mathbf{1}, \partial_t \mathbf{u}_i \rangle_H}_{\frac{d}{dt} \mathcal{U}_{ih}(t) = \frac{d}{dt} \langle \mathbf{1}, \mathbf{u}_i \rangle_H} + \underbrace{\langle \mathbf{1}, D \mathbf{f}_i \rangle_H}_{-\langle D \mathbf{1}, \mathbf{f}_i \rangle_H = 0} = \frac{\gamma_i}{2} \underbrace{\langle \mathbf{1}, (D_+ - D_-) \mathbf{g}_i \rangle_H}_{\langle (D_+ - D_-) \mathbf{1}, \mathbf{g}_i \rangle_H = 0}. \quad (76)$$

Then we have

$$\frac{d}{dt} \mathcal{U}_{ih}(t) = 0 \implies \mathcal{U}_{ih}(t) = \mathcal{U}_{ih}(0), \quad \forall t \geq 0, \quad (77)$$

which yields a conservative scheme. \square

The proof of entropy (nonlinear) stability for the semi-discrete approximation (74) does not necessarily follow. Following [50, 49], we can prove that the semi-discrete approximation (74) is linearly stable. We will formulate the result as the theorem.

Theorem 4.2. Consider the semi-discrete approximation (74) for a linear PDE flux, with $\mathbf{f} = A_x \mathbf{u}$ where $A_x \in \mathbb{R}^{m \times m}$ a symmetric (or symmetrisable) constant matrix and the periodic boundary conditions (65) implemented weakly through (71). For the classical global Lax-Friedrich flux splitting, that is if $\mathbf{g} = \mathbf{u}$ and $\gamma_i = \max_x |\max_j \lambda_j(A_x)|$, and the 3-tuple (D_-, D_+, H) satisfies the upwind DP SBP operator given by Assumptions (B.1)–(B.4) then we have

$$\partial_t \|\mathbf{u}\|_H^2 = \sum_{i=1}^m \gamma_i \langle \mathbf{u}_i, (D_+ - D_-) \mathbf{u}_i \rangle_H \leq 0, \quad \gamma_i = \max_j |\lambda_j(A_x)| > 0. \quad (78)$$

Proof. We set $\mathbf{f} = A_x \mathbf{u}$ where $A_x \in \mathbb{R}^{m \times m}$ a symmetric constant coefficients matrix and we proceed with the energy method. That is from the left, we multiply (74) with $\mathbf{u}^T (I_m \otimes H)$ and add the transpose of the product, and we have

$$\begin{aligned} \partial_t \|\mathbf{u}\|_H^2 &= - \underbrace{\langle (A_x \otimes D) \mathbf{u}, \mathbf{u} \rangle_H + \langle \mathbf{u}, (A_x \otimes D) \mathbf{u} \rangle_H}_{=0} + \sum_{i=1}^m \gamma_i \langle \mathbf{u}_i, (D_+ - D_-) \mathbf{u}_i \rangle_H \\ &= \sum_{i=1}^m \gamma_i \langle \mathbf{u}_i, (D_+ - D_-) \mathbf{u}_i \rangle_H \leq 0. \end{aligned}$$

\square

The linearly stable semi-discrete approximation (74) can be extended to multi-dimensional systems of nonlinear conservation laws by using different finite volume flux splitting techniques, [21, 4, 22], such as the classical global Lax-Friedrich flux splitting, Steger-Warming splitting, van Leer-Hänel splitting. Please see [50, 49] for more elaborate discussions.

In this study, we are particularly interested in provable nonlinear stable, conservative and high order accurate numerical approximations for systems of nonlinear hyperbolic conservation laws. As we will see from numerical experiments performed later in this paper, provably nonlinearly stable schemes can be more robust than their linearly stable counterparts.

4.2 The entropy-stable semi-discrete approximation

We now describe a method which yields a provably entropy stable, conservative, and high order accurate numerical method for systems of nonlinear conservation laws. The derived numerical method is robust and minimises spurious oscillations. The method combines three main ingredients: 1) the DP SBP operators, together with 2) skew-symmetric formulation, and 3) upwind flux splitting of nonlinear hyperbolic conservation laws so that the semi-discrete approximation is provably entropy-stable for arbitrary nonlinear system.

Again, for simplicity we consider the 1D conservation law,

$$\partial_t \mathbf{u} + \partial_x \mathbf{f}(\mathbf{u}) = 0 \iff \partial_t \mathbf{u} + \mathbf{F}(\mathbf{u}, \mathbf{f}(\mathbf{u}), \partial_x) = 0, \quad (79)$$

where $\mathbf{F}(\mathbf{u}, \mathbf{f}(\mathbf{u}), \partial_x) \equiv \partial_x \mathbf{f}(\mathbf{u})$ is the skew-symmetric form given in (32) and defined through (31) such that entropy stability can be proven using the energy method with only integration-by-parts, and without the chain/product rule.

We will begin with the following Lemma.

Lemma 4.3. Consider the semi-discrete approximation of the skew-symmetric form

$$\mathbf{F}(\mathbf{u}, \mathbf{f}(\mathbf{u}), D) \approx \mathbf{F}(\mathbf{u}, \mathbf{f}(\mathbf{u}), \partial_x), \quad (80)$$

where $D \approx \partial_x$ and $\mathbf{f}(\mathbf{u})$ is the PDE flux. If the 2-tuple (D, H) satisfies the traditional SBP operator given by Assumptions (A.1)–(A.3) then

$$\langle \mathbf{g}, \mathbf{F}(\mathbf{u}, \mathbf{f}(\mathbf{u}), D) \rangle_H = -\langle D\mathbf{1}, \mathbf{q} \rangle_H = 0.$$

where $\mathbf{g} \in \mathbb{R}^{mN}$ are the semi-discrete entropy variables and $\mathbf{q} \in \mathbb{R}^N$ is the semi-discrete entropy flux.

Next we introduce an upwind flux splitting (68) which will potentially yield entropy stability when upwinded. Specifically, we chose the entropy variables $\mathbf{g}_i = \partial_{\mathbf{u}_i} e(\mathbf{u})$, and $\gamma_i > 0$ are chosen such that \mathbf{f}_i and $\gamma_i \mathbf{g}_i$ have consistent units. Combining the skew-symmetric form and entropy stable upwind splitting with DP SBP operators yield the semi-discrete approximation

$$\partial_t \mathbf{u} + \mathbf{F}(\mathbf{u}, \mathbf{f}(\mathbf{u}), D) = \frac{1}{2} (\Gamma \otimes (D_+ - D_-)) \mathbf{g}, \quad D = \frac{1}{2} (D_+ + D_-), \quad (81)$$

where $\Gamma = \text{diag}([\gamma_1, \dots, \gamma_m])$, $\gamma_i > 0$. Note again that for smooth solutions the right hand side of (81) is very small, that is $|(\Gamma \otimes (D_+ - D_-)) \mathbf{g}| = O(\Delta x^{2p-1})$ where $p \geq 1$ is the order of accuracy of the discrete derivative operators D_\pm . For small enough Δx this term is much smaller than the truncation error $O(\Delta x^p)$. Next we will prove entropy stability. To begin, we approximate the total entropy (6) by the semi-discrete total entropy given by

$$E_h(t) := \langle \mathbf{1}, e \rangle_H. \quad (82)$$

The following definition, which is similar to the continuous analogue Definition 2.1, is central to this study.

Definition 4.1. Consider the semi-discrete approximation (81) and denote the semi-discrete total entropy $E_h(t) \geq 0$, defined by (82). The semi-discrete approximation (81) is called entropy-stable (entropy-conserving) if $E(t) \leq E_h(0)$ ($E_h(t) = E_h(0)$) for all $\mathbf{u} \in \mathbb{R}^{mN}$ and $t \in [0, T]$.

The first main theorem proves that the semi-discrete approximation (81) is entropy stable.

Theorem 4.4. Consider the semi-discrete approximation (81) where $\mathbf{F}(\mathbf{u}, \mathbf{f}(\mathbf{u}), D)$ is the semi-discrete approximation of the symmetric form with periodic boundary conditions. If $\mathbf{g}_i = \partial_{\mathbf{u}_i} e(\mathbf{u})$ and $\gamma_i > 0$, and the 3-tuple (D_-, D_+, H) satisfies the upwind DP SBP operator given by Assumptions (B.1)–(B.4), then the semi-discrete total entropy $E_h(t)$ satisfies

$$\frac{d}{dt} E_h(t) = \frac{1}{2} \sum_{i=1}^m \gamma_i \langle \mathbf{g}_i, (D_+ - D_-) \mathbf{g}_i \rangle_H \leq 0, \quad \gamma_i > 0. \quad (83)$$

Proof. Consider

$$\underbrace{\langle \mathbf{g}, \partial_t \mathbf{u} \rangle_H}_{\frac{d}{dt} E_h(t) = \frac{d}{dt} \langle \mathbf{1}, e \rangle_H} + \underbrace{\langle \mathbf{g}, \mathbf{F}(\mathbf{u}, \mathbf{f}(\mathbf{u}), D) \rangle_H}_{\langle \mathbf{1}, D\mathbf{q} \rangle_H = 0} = \frac{1}{2} \sum_{i=1}^m \gamma_i \langle \mathbf{g}_i, (D_+ - D_-) \mathbf{g}_i \rangle_H \leq 0. \quad (84)$$

Then we have

$$\frac{d}{dt} E_h(t) = \frac{1}{2} \sum_{i=1}^m \gamma_i \langle \mathbf{g}_i, (D_+ - D_-) \mathbf{g}_i \rangle_H \leq 0, \quad (85)$$

which yields an entropy dissipating (conserving) scheme for $\gamma_i > 0$ ($\gamma_i = 0$).

□

As in the continuous setting, we will give a few examples below.

Example 4.5. We consider the semi-discrete approximation of the Burgers' equation with the unknown u , the PDE flux $f(u) = u^2/2$, the entropy $e(u) = u^2/2$ and the entropy variable $g = \partial_u e(u) = u$. The skew-symmetric form of the divergence of the flux is

$$F(u, f(u), \partial_x) = \frac{1}{3} u \partial_x u + \frac{1}{3} \partial_x (u^2).$$

The upwind DP SBP semi-discrete approximation of the Burgers' is given by

$$\partial_t \mathbf{u} + \mathbf{F}(\mathbf{u}, \mathbf{f}(\mathbf{u}), D) = \frac{\gamma}{2} (D_+ - D_-) \mathbf{u}, \quad \gamma = |\mathbf{u}|_\infty > 0, \quad \mathbf{F}(\mathbf{u}, \mathbf{f}(\mathbf{u}), D) = \frac{1}{3} \mathbf{u} D \mathbf{u} + \frac{1}{3} D \mathbf{u}^2. \quad (86)$$

Since

$$\langle \mathbf{g}, \mathbf{F}(\mathbf{u}, \mathbf{f}(\mathbf{u}), D) \rangle_H = \frac{1}{3} \langle \mathbf{u}^2, D\mathbf{u} \rangle_H + \frac{1}{3} \langle \mathbf{u}, D\mathbf{u}^2 \rangle_H = 0,$$

it follows that

$$\frac{d}{dt} E_h(t) := \frac{1}{2} \frac{d}{dt} \|\mathbf{u}\|_H^2 = \frac{\gamma}{2} \langle \mathbf{u}, (D_+ - D_-) \mathbf{u} \rangle_H \leq 0. \quad (87)$$

Example 4.6. Now, consider the numerical approximation of the nonlinear shallow water equations in flux form, where the unknowns are $\mathbf{U} = (h, uh)^T$ and skew-symmetric PDE flux and the entropy variables are given by

$$\mathbf{F}(\mathbf{U}, \mathbf{f}(\mathbf{U}), \partial_x) = \begin{bmatrix} \partial_x(hu) \\ \frac{1}{2} \partial_x(hu^2) + \frac{1}{2} u \partial_x(hu) + \frac{1}{2} hu \partial_x u + gh \partial_x h \end{bmatrix}, \quad \mathbf{g} = \begin{bmatrix} gh - \frac{1}{2} u^2 \\ u \end{bmatrix}. \quad (88)$$

An upwind DP SBP method for the nonlinear shallow water equations in flux form is given by

$$\partial_t \mathbf{U} + \mathbf{F}(\mathbf{U}, \mathbf{f}(\mathbf{U}), D) = \frac{1}{2} (\Gamma \otimes (D_+ - D_-)) \mathbf{g}, \quad \Gamma = \begin{bmatrix} \gamma_1 & 0 \\ 0 & \gamma_2 \end{bmatrix}, \quad \gamma_1, \gamma_2 \geq 0, \quad (89)$$

where

$$\mathbf{F}(\mathbf{U}, \mathbf{f}(\mathbf{U}), D) = \begin{bmatrix} D(hu) \\ \frac{1}{2} D(hu^2) + \frac{1}{2} u D(hu) + \frac{1}{2} (hu) D u + gh D h \end{bmatrix}, \quad \mathbf{g} = \begin{bmatrix} gh - \frac{1}{2} u^2 \\ u \end{bmatrix}. \quad (90)$$

It is easy to check that

$$\langle \mathbf{g}, \mathbf{F}(\mathbf{U}, \mathbf{f}(\mathbf{U}), D) \rangle_H = \langle gh, D(hu) \rangle_H + \langle uh, D(gh) \rangle_H + \frac{1}{2} \langle \mathbf{u}, D(hu^2) \rangle_H + \frac{1}{2} \langle hu^2, D u \rangle_H = 0.$$

Then it follows that

$$\frac{d}{dt} E_h(t) = \frac{1}{2} \langle \mathbf{g}, (\Gamma \otimes (D_+ - D_-)) \mathbf{g} \rangle_H = \frac{1}{2} \sum_{i=1}^2 \gamma_i \langle \mathbf{g}_i, (D_+ - D_-) \mathbf{g}_i \rangle_H \leq 0. \quad (91)$$

If $\gamma_1 = \gamma_2 = 0$ for all $t \geq 0$, then we have conservation of entropy, that is $E_h(t) = E_h(0)$ for all $t \geq 0$.

4.3 Numerical conservation properties

We will show that our semi-discrete scheme (81) is conservative. Conservative properties of the scheme will be important in proving the convergence of the numerical method for nonlinear problems with weak solutions [3, 4]. In particular, we will show that (81) satisfies the discrete equivalence of (34)–(35) and preserves some other important invariants present in the continuous model. We will conclude by giving the 1D model examples, the Burger's equation and the nonlinear shallow water equations.

We will now prove the discrete equivalence of (34)–(35).

Lemma 4.7. Consider the semi-discrete approximation of the skew-symmetric form

$$\mathbf{F}(\mathbf{u}, \mathbf{f}(\mathbf{u}), D) \approx \mathbf{F}(\mathbf{u}, \mathbf{f}(\mathbf{u}), \partial_x), \quad (92)$$

where $D \approx \partial_x$ and $\mathbf{f}(\mathbf{u})$ is the PDE flux and $\mathbf{F}(\mathbf{u}, \mathbf{f}(\mathbf{u}), \partial_x)$ is skew-symmetric form of the divergence of the flux satisfying (34). If the 2-tuple (D, H) satisfies the traditional SBP operator given by Assumptions (A.1)–(A.3) and the periodic boundary conditions are implemented weakly through (71) then

$$\langle \mathbf{1}, \mathbf{F}_i(\mathbf{u}, \mathbf{f}(\mathbf{u}), D) \rangle_H = -\langle D\mathbf{1}, \mathbf{f}_i \rangle_H = 0, \quad \forall i = 1, 2, \dots, m,$$

where $\mathbf{f}_i \in \mathbb{R}^N$ are the semi-discrete PDE fluxes restricted on the grid.

The second main theorem proves that the DP-SBP approximation (81) is globally conservative.

Theorem 4.8. Consider the semi-discrete upwind DP-SBP approximation (81) where $\mathbf{F}(\mathbf{u}, \mathbf{f}(\mathbf{u}), D)$ is the semi-discrete approximation of the symmetric form with periodic boundary conditions implemented weakly through (71). If Lemma 4.7 holds and the 3-tuple (D_-, D_+, H) satisfies the upwind DP SBP operator given by Assumptions (B.1)–(B.4), then the semi-discrete total quantity $\mathcal{U}_{ih}(t) = \langle \mathbf{1}, \mathbf{u}_i \rangle_H$ satisfies

$$\frac{d}{dt} \mathcal{U}_{ih}(t) = \langle D\mathbf{1}, \mathbf{f}_i \rangle_H + \frac{\gamma_i}{2} \langle (D_+ - D_-) \mathbf{1}, \mathbf{g}_i \rangle_H = 0, \quad \gamma_i \geq 0. \quad (93)$$

Proof. For all $i = 1, 2, \dots, m$, we consider

$$\underbrace{\langle \mathbf{1}, \partial_t \mathbf{u}_i \rangle_H}_{\frac{d}{dt} \mathcal{U}_{ih}(t) = \frac{d}{dt} \langle \mathbf{1}, \mathbf{u}_i \rangle_H} + \underbrace{\langle \mathbf{1}, \mathbf{F}_i(\mathbf{u}, \mathbf{f}(\mathbf{u}), D) \rangle_H}_{-\langle D\mathbf{1}, \mathbf{f}_i \rangle_H = 0} = \frac{\gamma_i}{2} \underbrace{\langle \mathbf{1}, (D_+ - D_-) \mathbf{g}_i \rangle_H}_{\langle (D_+ - D_-) \mathbf{1}, \mathbf{g}_i \rangle_H = 0}. \quad (94)$$

Then we have

$$\frac{d}{dt} \mathcal{U}_{ih}(t) = 0 \implies \mathcal{U}_{ih}(t) = \mathcal{U}_{ih}(0), \quad \forall t \geq 0, \quad (95)$$

which yields a conservative scheme. \square

Thus, by construction, the semi-discrete upwind DP-SBP approximation (81) is conservative and entropy stable for arbitrary nonlinear conservation law in skew-symmetric form. We will give some examples below to verify the conservative properties of the scheme.

Example 4.9. Consider the semi-discretisation approximation (86) of the Burgers' equation. We will show that the total "mass" is semi-discretely conserved, as in the continuous equation. Consider the time derivative of the total "mass", we have

$$\partial_t \langle \mathbf{1}, \mathbf{u} \rangle_H = \langle \mathbf{1}, \partial_t \mathbf{u} \rangle_H = -\frac{1}{3} \langle \mathbf{1}, \mathbf{u} D \mathbf{u} \rangle_H - \frac{1}{3} \langle \mathbf{1}, D \mathbf{u}^2 \rangle_H + \frac{\gamma}{2} \langle \mathbf{1}, (D_+ - D_-) \mathbf{u} \rangle_H.$$

With the fact that H is diagonal we have

$$\begin{aligned} \partial_t \langle \mathbf{1}, \mathbf{u} \rangle_H &= -\frac{1}{3} \langle \mathbf{u}, D \mathbf{u} \rangle_H - \frac{1}{3} \langle \mathbf{1}, D \mathbf{u}^2 \rangle_H + \frac{\gamma}{2} \langle \mathbf{1}, (D_+ - D_-) \mathbf{u} \rangle_H \\ &= -\frac{1}{6} (\langle \mathbf{u}, D \mathbf{u} \rangle_H + \langle \mathbf{u}, D \mathbf{u} \rangle_H) - \frac{1}{3} \langle \mathbf{1}, D \mathbf{u}^2 \rangle_H + \frac{\gamma}{2} \langle \mathbf{1}, (D_+ - D_-) \mathbf{u} \rangle_H. \end{aligned}$$

Using the SBP property we have

$$\partial_t \langle \mathbf{1}, \mathbf{u} \rangle_H = -\frac{1}{6} (\langle D \mathbf{u}, \mathbf{u} \rangle_H - \langle \mathbf{u}, D \mathbf{u} \rangle_H) - \frac{1}{3} \langle \mathbf{1}, D \mathbf{u}^2 \rangle_H + \frac{\gamma}{2} \langle (D_+ - D_-) \mathbf{1}, \mathbf{u} \rangle_H = 0.$$

Example 4.10. Next, we consider the semi-discrete approximation (89) of the nonlinear shallow water equation. We will show (89) semi-discretely conserves mass and momentum.

To begin, we consider the time derivative of the total mass,

$$\partial_t \langle \mathbf{1}, \mathbf{h} \rangle_H = \langle \mathbf{1}, \partial_t \mathbf{h} \rangle_H = -\left\langle \mathbf{1}, D(\mathbf{h} \mathbf{u}) + \frac{\gamma_1}{2} (D_- - D_+) \mathbf{u} \right\rangle_H,$$

Using the DP SBP properties, we have

$$\partial_t \langle \mathbf{1}, \mathbf{h} \rangle_H = \langle D \mathbf{1}, \mathbf{h} \mathbf{u} \rangle_H + \frac{\gamma_1}{2} \langle (D_- - D_+) \mathbf{1}, \mathbf{u} \rangle_H = 0.$$

Similarly, we show that the semi-discrete approximation (89) semi-discretely conserves momentum. We take the time derivative of the total momentum,

$$\begin{aligned} \partial_t \langle \mathbf{1}, \mathbf{h} \mathbf{u} \rangle_H &= \langle \mathbf{1}, \partial_t (\mathbf{h} \mathbf{u}) \rangle_H = -\left\langle \mathbf{1}, \frac{1}{2} D(\mathbf{h} \mathbf{u}^2) + \frac{1}{2} \mathbf{u} D(\mathbf{h} \mathbf{u}) + \frac{1}{2} \mathbf{h} \mathbf{u} D \mathbf{u} + g \mathbf{h} D \mathbf{h} \right\rangle_H \\ &\quad - \frac{\gamma_2}{2} \left\langle \mathbf{1}, (D_- - D_+) \left(g \mathbf{h} - \frac{1}{2} \mathbf{u}^2 \right) \right\rangle_H \\ &= \left\langle \mathbf{1}, \frac{1}{2} \mathbf{u} D(\mathbf{h} \mathbf{u}) + \frac{1}{2} (\mathbf{h} \mathbf{u}) D \mathbf{u} + g \mathbf{h} D \mathbf{h} \right\rangle_H \\ &= \frac{1}{2} \langle D \mathbf{u}, \mathbf{h} \mathbf{u} \rangle_H - \frac{1}{2} \langle \mathbf{h} \mathbf{u}, D \mathbf{u} \rangle_H - \frac{g}{2} \langle \mathbf{h}, D \mathbf{h} \rangle_H + \frac{g}{2} \langle D \mathbf{h}, \mathbf{h} \rangle_H = 0. \end{aligned}$$

The analysis extends to 2D and 3D, and to the Euler equations of gas dynamics. Below, we provide a few remarks to compare and contrast the proposed method (81) with traditional and state-of-the-art methods.

Remark 3. The main difference between the proposed method (81) and traditional and recent state-of-the-art methods developed in the literature such as [6, 7, 8] is the term in the right hand side of (81) which controls grid-scale oscillations. For smooth solutions, $\mathbf{u} \in C^1(\Omega \times [0, T])$, the term in the right hand side of (81) is proportional to $O(\Delta x^{2p-1})$, and for $p > 1$ is much less than the truncation error $O(\Delta x^p)$ which can be small for smooth solutions and resolved meshes. However, for unresolved meshes and non-smooth solutions, $\mathbf{u} \notin C^1(\Omega \times [0, T])$, the term on the right hand side of (81) can be significant and will dissipate entropy when $\gamma_i > 0$.

Remark 4. We elaborate on the efficiency of the proposed method (81). Note that the term in the right hand side of (81) can be (mistakenly) related to artificial hyper-viscosity operator applied to the entropy variable g . However, the discrete operator consists of the difference of the first derivative DP SBP operators which is efficient to evaluate. This is opposed to the traditional and state-of-the-art artificial hyper-viscosity operators [58, 9, 10, 11, 12] that require the evaluation high even-order spatial derivative operators $\sim \partial^{2p}/\partial x^{2p}$, $p \geq 1$, which can be computationally expensive, compromise conservation of important invariant and would often further limit explicit time-steps for the fully discrete problem.

Remark 5. The term in the right hand side of (81) is a penalty on the discrete gradient of the solution (entropy variables) at every grid point which weakly ensures smoothness and measures unresolved features in the numerical solution. Again, for smooth solutions, $\mathbf{u} \in C^1(\Omega \times [0, T])$, this term is small and will vanish in the limit of mesh refinement. However, for unresolved meshes and non-smooth solutions, $\mathbf{u} \notin C^1(\Omega \times [0, T])$, the term can be significant and will decimate grid-scale errors. Therefore, the proposed numerical framework has an inbuilt "limiter" whose goal is to detect and effectively resolve regions where the solution is poorly resolved and/or discontinuities are found. Numerical experiments performed later in this paper corroborates the analysis.

Remark 6. The proposed DP SBP FD method (81) is structurally equivalent to entropy-stable DG methods develop in the literature such as [13, 14, 15, 16, 17, 18, 19]. However, the DP SBP operators are designed to be upwind, that is they come with some built-in dissipation everywhere, as opposed to DG methods for hyperbolic PDEs which can only induce dissipation through numerical fluxes acting at element interfaces.

In the next section, we will present some numerical experiments to verify the analysis and demonstrate the robustness of our numerical framework.

5 Numerical results

In this section, we present numerical experiments to validate the theoretical analysis presented in the previous sections. In particular, the numerical experiments are designed to verify accuracy, stability, robustness and the improvements of the framework over the state-of-the-art methods.

The numerical methods are implemented in the Julia programming language [59]. Unless stated otherwise, the numerical experiments are carried out using the DP SBP operators [47] of interior order of accuracy 4,5,6, and 7, provided in the Julia package *SummationByPartsOperators.jl* [60]. As discussed earlier, we will only consider periodic boundary conditions imposed weakly using penalty terms. For the time integration, we use the explicit 5 stage 4th-order accurate strong stability preserving Runge-Kutta (SSP RK) method of [61] provided by the Julia package *OrdinaryDiffEq.jl* [62]. All figures in the following numerical experiments are generated using the Julia package *Makie.jl* [63] or *Paraview* [64].

The numerical experiments will be conducted with increasing complexity. That is, first we consider the 1D Burger's equation, second we consider the (1D and 2D) nonlinear shallow water equations, and finally the (1D and 2D) compressible Euler equations of gas dynamics are considered. We will regularly compare the linearly stable semi-discrete approximation (74), with global Lax-Friedrichs flux splitting, against the entropy-conservative scheme (81) with $\gamma = 0$ and the entropy-stable scheme (81) with $\gamma > 0$. It is also important to note that no artificial viscosity, limiting or filtering is used throughout the numerical simulations.

5.1 The inviscid Burgers' equation

We begin with the 1D inviscid Burger's equation (10) and verify numerical accuracy. We force the equation (10) to satisfy the manufactured (exact) solution

$$u = 2 + 0.3 \sin(2\pi(x - t)), \quad x \in [-1, 1]. \quad (96)$$

We set the final time of $t = 2$ with a time-step of $\Delta t = 0.1\Delta x$, and run the simulations on a sequence of increasing mesh resolutions $\Delta x > 0$. Figure 3 and Table 2 show the error and the convergence of the error at the final time $t = 2$, for the different schemes. Note that the convergence rates of the errors are slightly better than the expected theoretical rates shown in Table 1.

To investigate how the schemes handle non-smooth solutions, we consider the Gaussian initial data,

$$u(x, 0) = \exp(-(x - 0.25)^2/0.01),$$

the spatial domain $\Omega = [0, 1]$ discretized with $n = 256$ grid points and evolve the numerical solutions until $t = 1$. The snapshots of the solutions are shown in Figure 1. The total entropy/energy $E_h(t)$ and the total conserved quantity

$\mathcal{U}_h(t) = \langle \mathbf{1}, \mathbf{u} \rangle_H$ are shown in Figure 2. Note that the entropy-conserving scheme, (81) with $\gamma = 0$, conserves both $E_h(t)$ and $\mathcal{U}_h(t)$ up to rounding errors. However, the entropy conserving scheme supports wildly oscillatory numerical solutions, which pollute the simulation when shocks develop. The linearly stable DP SBP method (74) and our entropy-stable method (81), with $\gamma = |\mathbf{u}(t)|_\infty > 0$, conserve $\mathcal{U}_h(t)$ up to rounding errors and tame the wildly oscillatory solutions. It is also noteworthy that total entropy is conserved initially when the solution is smooth, and is dissipated when shocks develop. This is in agreement with (81) with $\gamma = |\mathbf{u}(t)|_\infty > 0$ as shown in Theorem 4.4. The Burger's equation, although being a simple 1D model problem, clearly demonstrates the important numerical properties of our proposed entropy stable DP SBP framework, (81), with $\gamma = |\mathbf{u}(t)|_\infty > 0$. In the next sections, we will see how these properties carry over to more complicated models of the nonlinear shallow water equations and the compressible Euler's equation of gas dynamics.

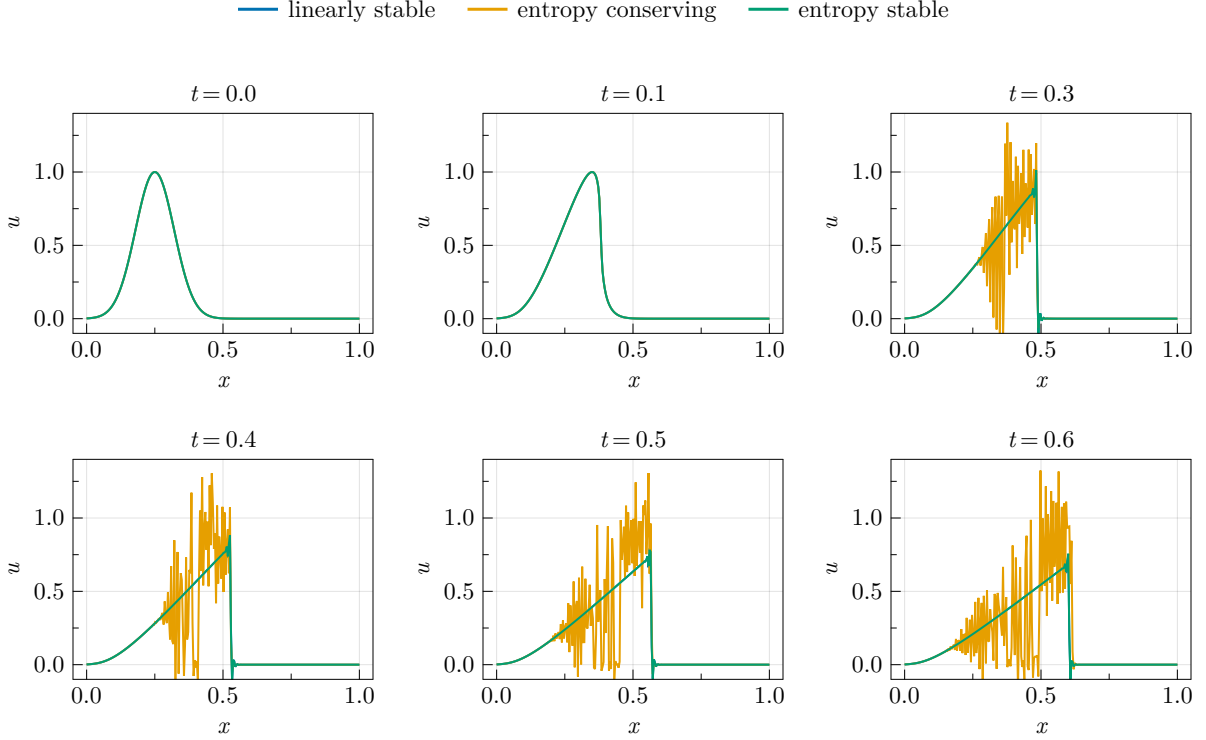


Figure 1: Snapshots of the solution \mathbf{u} at $t = 0.0, 0.1, 0.3$. Note that the entropy-conserving scheme, $\gamma = 0$, support oscillatory solutions at the shock. The linearly stable DP method and our entropy-stable method, $\gamma = |\mathbf{u}(t)|_\infty > 0$, tames the wildly oscillatory solutions.

5.2 The shallow water equations

Next, we consider the nonlinear shallow water equations in 1D and 2D. The 2D skew-symmetric form and the semi-discrete approximation is given in Appendix A. To begin, we will perform numerical experiments to verify accuracy and well-balance properties. Then we will demonstrate robustness by simulating 2D flow problems which will include the merging vortices [35, 65] and the barotropic shear instability [35, 66, 67], with fully developed turbulence.

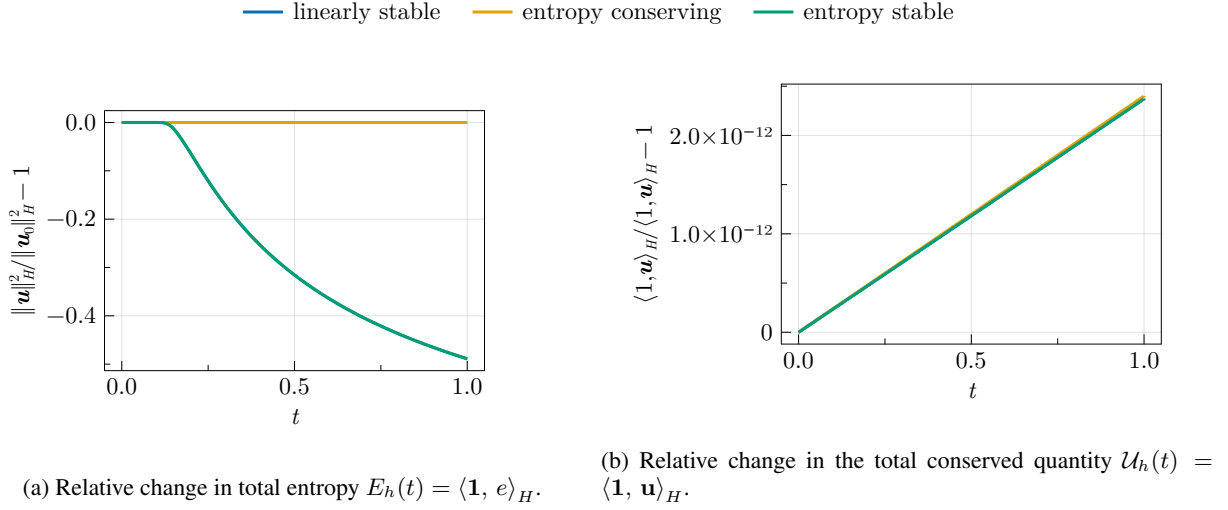
5.2.1 Convergence tests for the shallow water equation

To verify accuracy, we force the 1D shallow water equations to satisfy the manufactured (exact) solution

$$h = 2 + 0.3 \sin(2\pi(x - t)), \quad u = 2 + 0.3 \sin(2\pi(x + t)), \quad x \in [-1, 1]. \quad (97)$$

The manufactured solution for the 2D shallow water equations is

$$h = 2 + 0.2 \sin(2\pi(x - t)) \sin(2\pi(y - t)), \quad u = v = 2 + 0.2 \sin(2\pi(x + t)) \sin(2\pi(y + t)), \quad (x, y) \in [-1, 1]^2. \quad (98)$$

Figure 2: Relative change in total entropy $E_h(t)$ and total conserved quantity $U_h(t)$ for the 1D Burger's equation.

N	linearly stable		entropy conserving		entropy stable		N	linearly stable		entropy conserving		entropy stable	
	Error	EOC	Error	EOC	Error	EOC		Error	EOC	Error	EOC	Error	EOC
32	1.93e-03	-	2.75e-03	-	1.75e-03	-	32	1.70e-03	-	4.48e-03	-	1.54e-03	-
64	1.56e-04	3.55	1.87e-04	3.79	1.48e-04	3.49	64	1.34e-04	3.58	3.16e-04	3.74	1.27e-04	3.52
128	1.33e-05	3.51	1.80e-05	3.34	1.29e-05	3.47	128	1.10e-05	3.57	2.50e-05	3.62	1.07e-05	3.53
256	1.10e-06	3.57	1.63e-06	3.44	1.09e-06	3.55	256	9.06e-07	3.58	1.88e-06	3.71	8.96e-07	3.56
512	9.40e-08	3.54	1.42e-07	3.51	9.33e-08	3.53	512	7.84e-08	3.52	1.50e-07	3.64	7.80e-08	3.51

(a) interior order of accuracy 4

(b) interior order of accuracy 5

N	linearly stable		entropy conserving		entropy stable		N	linearly stable		entropy conserving		entropy stable	
	Error	EOC	Error	EOC	Error	EOC		Error	EOC	Error	EOC	Error	EOC
32	6.10e-04	-	9.10e-04	-	5.80e-04	-	32	7.03e-04	-	8.70e-04	-	6.79e-04	-
64	3.34e-05	4.10	9.01e-05	3.26	2.25e-05	4.58	64	3.83e-05	4.10	1.68e-04	2.32	2.62e-05	4.59
128	2.00e-06	4.02	2.50e-06	5.11	1.27e-06	4.10	128	2.23e-06	4.06	3.12e-06	5.69	1.42e-06	4.16
256	9.60e-08	4.35	3.36e-07	2.88	6.24e-08	4.33	256	1.07e-07	4.36	2.04e-07	3.91	6.94e-08	4.33
512	4.35e-09	4.45	2.38e-08	3.81	2.87e-09	4.43	512	4.85e-09	4.45	1.98e-08	3.36	3.19e-09	4.43

(c) interior order of accuracy 6

(d) interior order of accuracy 7

Table 2: Convergence rates for the l^2 error at final time $t = 2$ for the 1D Burger's equation.

In 1D the penalty weights for discrete derivative operators are given by

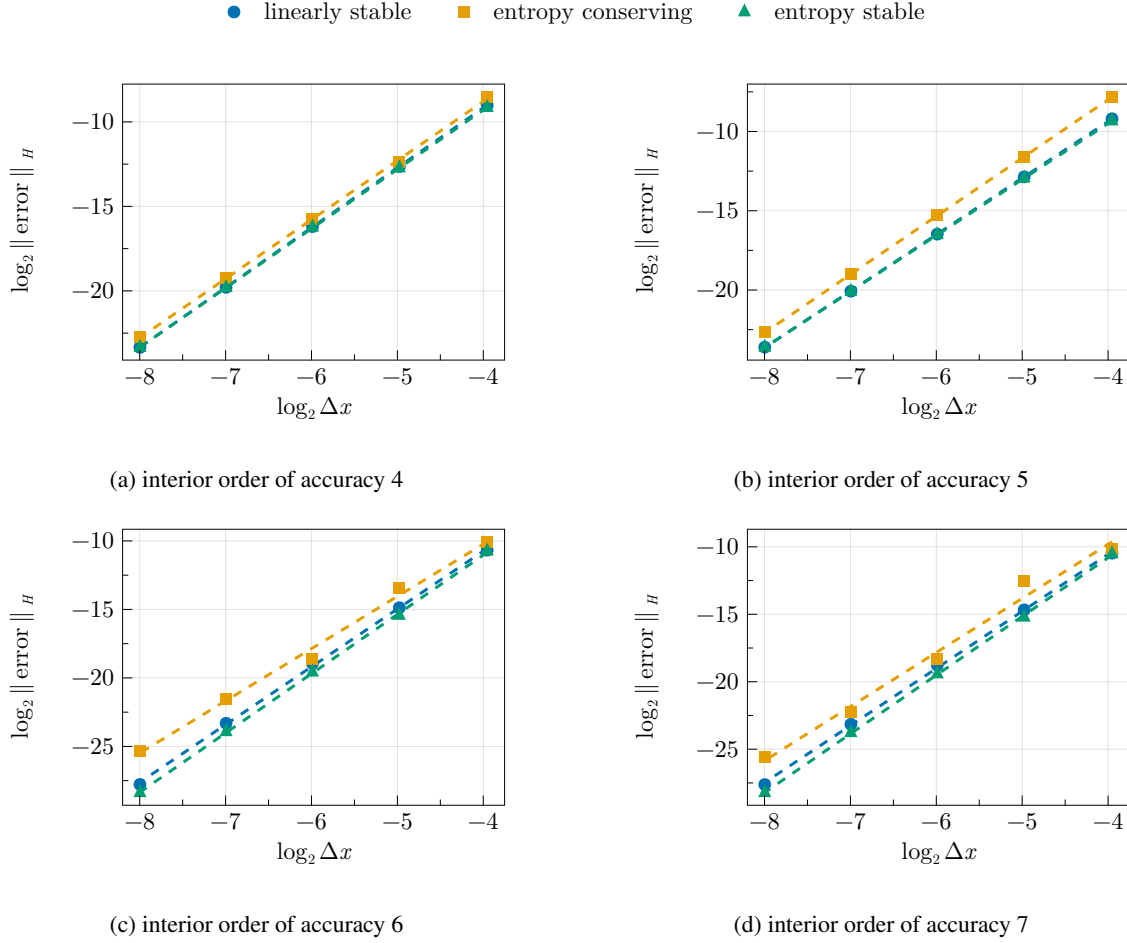
$$\Gamma = \text{diag} \left(\left[2 \max_x \frac{h}{c}, 4 \max_x \left(h \left(c - \frac{1}{2} \sqrt{gh} \right) \right) \right] \right), \quad c = |u| + \sqrt{gh} > 0. \quad (99)$$

The numerical method for the 2D shallow water equation is briefly discussed in Appendix A.

We integrate the numerical solution until the final time $t = 2$, on a sequence of increasing mesh resolutions, with the time-step $\Delta t = 0.1/d \times \Delta x$, where $d \in \{1, 2\}$ is the spatial dimension. Figure 4 and Table 3 show the numerical errors and the convergence of the errors at the final time $t = 2$ for the 1D shallow water equations. Similarly, Figure 5 and Table 4 show the numerical errors and the convergence of the errors at the final time $t = 2$ for the 2D shallow water equation. As above, note that the recorded numerical convergence rates of the numerical errors are slightly better than the expected theoretical rates shown in Table 1.

5.2.2 Well-Balanced

A desirable property for a numerical method for conservation laws is preserving steady state solutions. This property is known as well-balancedness for the shallow water equations. We test our scheme on the 1D lake at rest model with an immersed bump steady state problem using the 1D shallow water equations with bottom topography as described in [68, 35]. We consider the spatial domain $[0, 25]$ with periodic boundary conditions and a bottom topography

Figure 3: The l^2 numerical errors at $t = 2$ for the 1D Burger's equation.

described by

$$b(x) = \begin{cases} 0.2 - 0.05(x - 10)^2 & \text{if } 8 < x < 12 \\ 0 & \text{otherwise.} \end{cases} \quad (100)$$

The initial conditions are a steady state solution given as

$$\begin{aligned} h_0(x) &= 0.5 - b(x) \\ u_0(x) &= 0. \end{aligned}$$

The steady state solution is illustrated in Figure 6. Note that we can prove that our semi-discrete scheme is perfectly well-balanced for steady-state solutions with zero velocity, but we omit this for brevity. Thus, we expect our method to achieve machine-precision rounding error for the lake at rest problem. Indeed, the numerical errors we observe in Table 5 are within the machine-precision rounding errors.

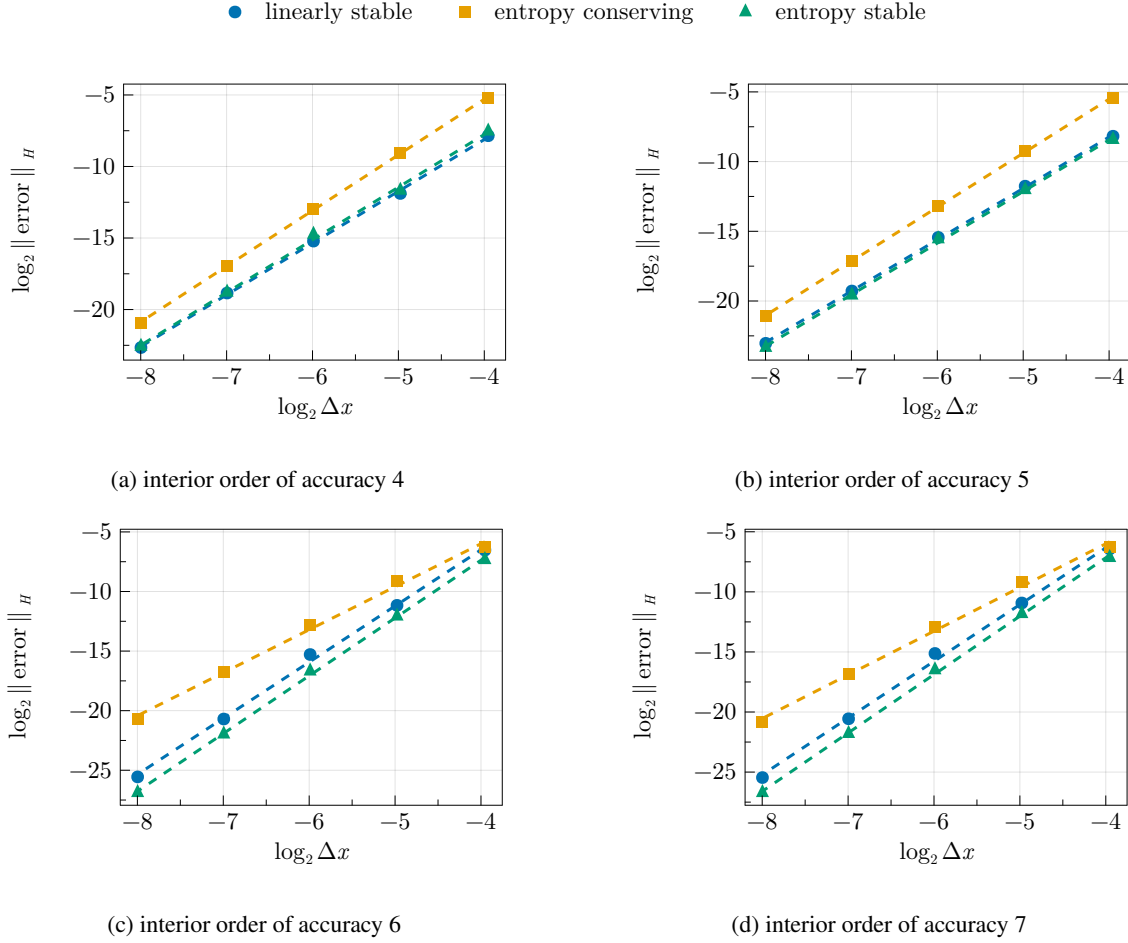
5.2.3 The 2D merging vortices

Next we consider the merging vortices [65, 35], modeled by the 2D rotating nonlinear shallow water equations in the doubly periodic spatial domain $\Omega = [0, 2\pi] \times [0, 2\pi]$. The initial conditions are a pair of Gaussian vortices ψ_+ , ψ_- with the incompressible stream function $\psi = \psi_+ + \psi_-$, defined by

$$\psi_-(x, y) = e^{-2.5((x - (3.05 - 0.45)\pi/3)^2 + (y - \pi)^2)}, \quad \psi_+(x, y) = e^{-2.5((x - (3.05 + 0.45)\pi/3)^2 + (y - \pi)^2)}. \quad (101)$$

To ensure linear geostrophic balance $f\mathbf{u}^\perp + g\nabla h = 0$, we set the initial conditions

$$h_0(x, y) = H + \frac{f}{g}\psi(x, y), \quad u_0(x, y) = -\partial_y\psi(x, y), \quad v_0(x, y) = \partial_x\psi(x, y), \quad (102)$$

Figure 4: The l^2 numerical errors at $t = 2$ for the 1D shallow water equations.

where we have chosen the numerical values of the parameters to be $f = g = 5$, $H = 8$. The initial condition for potential vorticity is plotted in Figure 7a.

For smooth solutions, nonlinear conservation laws preserve infinitely many invariants. However, any discrete approximation can (approximately) preserve a finite number of invariants [34, 35] and when solutions are non-smooth some of the invariants would be dissipated or amplified by the physical system and numerical schemes. For our numerical simulation of the nonlinear shallow water equations, in addition to the total quantity $\mathcal{U}(t)$, we select a subset of the invariants, namely: 1) total energy/entropy $E(t)$, 2) total enstrophy $E_s(t)$, 3) total absolute vorticity $W(t)$ and 4) total mass $M(t)$, defined by

$$E(t) = (1, e), \quad E_s(t) = (1, \mathcal{E}), \quad W(t) = (1, \omega), \quad M(t) = (1, h), \quad (103)$$

which the numerical method should accurately preserve. Here, $e = \frac{1}{2}(gh^2 + hu^2 + hv^2)$ is the entropy, $\omega = \partial_x v - \partial_y u + f$ is the absolute vorticity, f is the Coriolis parameter and $\mathcal{E} = h^{-1}\omega^2$ is the enstrophy density. While the total entropy $E(t)$ is critical for nonlinear stability and the total enstrophy E_s is a higher order moment and weakly bounds the derivatives of the solution. Therefore, total entropy and total enstrophy must not grow with time, and are crucial for numerical stability, controlling grid-scale errors. In particular, controlling the total enstrophy E_s would ensure that high frequency oscillations do not overwhelm numerical solutions.

We discretise the spatial domain using 128×128 grid points and evolve the numerical solution until the final time $t = 20$ with the time-step $\Delta t = (0.1/d)\Delta x$. The numerical approximations of the invariants are given by

$$E_h(t) = \langle \mathbf{1}, e \rangle_H, \quad E_{sh}(t) = \langle \mathbf{1}, \mathcal{E} \rangle_H, \quad W_h(t) = \langle \mathbf{1}, \omega \rangle_H, \quad M_h(t) = \langle \mathbf{1}, h \rangle_H. \quad (104)$$

N	linearly stable		entropy conserving		entropy stable		N	linearly stable		entropy conserving		entropy stable	
	Error	EOC	Error	EOC	Error	EOC		Error	EOC	Error	EOC	Error	EOC
32	4.33e-03	-	2.72e-02	-	5.39e-03	-	32	3.45e-03	-	2.30e-02	-	2.91e-03	-
64	2.64e-04	3.94	1.91e-03	3.75	3.07e-04	4.04	64	2.88e-04	3.50	1.68e-03	3.70	2.41e-04	3.52
128	2.63e-05	3.29	1.24e-04	3.89	3.63e-05	3.04	128	2.25e-05	3.63	1.10e-04	3.89	2.08e-05	3.49
256	2.12e-06	3.61	7.98e-06	3.94	2.20e-06	4.02	256	1.57e-06	3.82	6.92e-06	3.96	1.27e-06	4.01
512	1.51e-07	3.80	5.06e-07	3.97	1.60e-07	3.78	512	1.16e-07	3.74	4.52e-07	3.93	9.43e-08	3.74

(a) interior order of accuracy 4

N	linearly stable		entropy conserving		entropy stable		N	linearly stable		entropy conserving		entropy stable	
	Error	EOC	Error	EOC	Error	EOC		Error	EOC	Error	EOC	Error	EOC
32	1.09e-02	-	1.27e-02	-	6.19e-03	-	32	1.17e-02	-	1.32e-02	-	7.02e-03	-
64	4.37e-04	4.53	1.78e-03	2.77	2.32e-04	4.63	64	5.14e-04	4.40	1.68e-03	2.91	2.77e-04	4.56
128	2.50e-05	4.08	1.38e-04	3.65	9.49e-06	4.56	128	2.80e-05	4.15	1.28e-04	3.67	1.08e-05	4.62
256	5.87e-07	5.38	9.07e-06	3.91	2.43e-07	5.26	256	6.46e-07	5.41	8.53e-06	3.89	2.74e-07	5.27
512	2.02e-08	4.84	5.79e-07	3.96	8.07e-09	4.90	512	2.17e-08	4.88	5.47e-07	3.95	9.07e-09	4.90

(b) interior order of accuracy 5

(c) interior order of accuracy 6

(d) interior order of accuracy 7

Table 3: The convergence of the l^2 numerical errors at $t = 2$ for the 1D shallow equations.

N	linearly stable		entropy conserving		entropy stable		N	linearly stable		entropy conserving		entropy stable	
	Error	EOC	Error	EOC	Error	EOC		Error	EOC	Error	EOC	Error	EOC
32	3.86e-03	-	4.77e-03	-	5.14e-03	-	32	2.43e-03	-	6.89e-03	-	3.21e-03	-
64	2.47e-04	3.88	3.87e-04	3.54	4.33e-04	3.49	64	1.63e-04	3.81	4.15e-04	3.96	2.47e-04	3.61
128	2.03e-05	3.56	2.53e-05	3.89	4.34e-05	3.28	128	1.46e-05	3.43	2.84e-05	3.82	2.69e-05	3.16
256	1.44e-06	3.80	1.88e-06	3.73	3.52e-06	3.60	256	1.05e-06	3.77	1.80e-06	3.96	1.56e-06	4.08

(a) interior order of accuracy 4

N	linearly stable		entropy conserving		entropy stable		N	linearly stable		entropy conserving		entropy stable	
	Error	EOC	Error	EOC	Error	EOC		Error	EOC	Error	EOC	Error	EOC
32	1.82e-03	-	4.49e-03	-	1.67e-03	-	32	1.93e-03	-	7.91e-03	-	1.92e-03	-
64	1.57e-04	3.45	2.19e-04	4.26	8.58e-05	4.18	64	1.71e-04	3.42	3.09e-04	4.57	8.98e-05	4.32
128	5.49e-06	4.79	1.40e-05	3.92	3.14e-06	4.72	128	6.03e-06	4.77	1.99e-05	3.91	3.55e-06	4.61
256	2.56e-07	4.40	9.05e-07	3.93	1.26e-07	4.62	256	2.82e-07	4.40	1.03e-06	4.25	1.45e-07	4.59

(b) interior order of accuracy 5

(c) interior order of accuracy 6

(d) interior order of accuracy 7

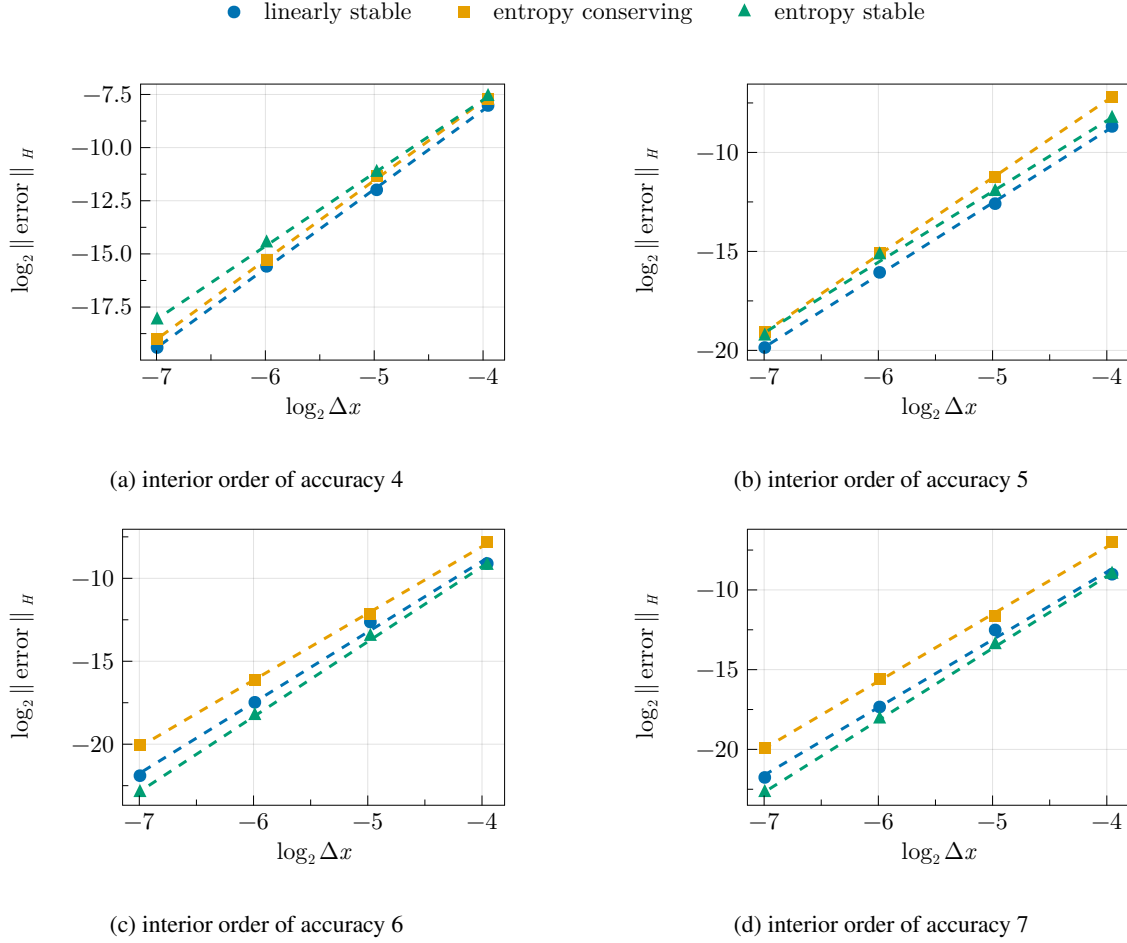
Table 4: The convergence of the l^2 numerical errors at $t = 2$ for the 2D shallow equations.

The snapshots of the potential vorticity ω/h are shown in Figure 8, where we also compare our entropy-stable DP-SBP framework with the the state-of-the-art entropy conserving split-form SBP method. Our entropy stable DP-SBP framework remains stable and preserves the structures of the vortices. However, the state-of-the-art entropy conserving method generates large grid-scale numerical oscillations which destroys the structure of the vortices, and could eventually crash the simulation.

N	interior order 4				N	interior order 5			
	32	64	128	256		32	64	128	256
linearly stable	2.41e-13	4.92e-13	9.99e-13	2.00e-12	2.43e-13	4.91e-13	1.00e-12	2.01e-12	
entropy conserving	2.40e-13	4.79e-13	9.66e-13	1.93e-12	2.41e-13	4.81e-13	9.64e-13	1.94e-12	
entropy stable	2.42e-13	4.92e-13	9.95e-13	1.99e-12	2.43e-13	4.95e-13	1.00e-12	2.01e-12	

N	interior order 6				N	interior order 7			
	32	64	128	256		32	64	128	256
linearly stable	2.40e-13	4.89e-13	9.91e-13	1.98e-12	2.42e-13	4.89e-13	1.00e-12	2.01e-12	
entropy conserving	2.43e-13	4.78e-13	9.63e-13	1.92e-12	2.42e-13	4.83e-13	9.75e-13	1.94e-12	
entropy stable	2.37e-13	4.79e-13	9.71e-13	1.95e-12	2.43e-13	4.91e-13	1.00e-12	2.01e-12	

Table 5: Relative maximum numerical error of the lake at rest problem at $t = 20$, where N is the number of grid points. Note that the numerical errors are trivial up to rounding errors independent of mesh resolution.

Figure 5: The l^2 numerical errors at $t = 2$ for the 2D shallow equations.

We have also plotted the relative changes of the numerical invariants with time, see Figure 9. Note that both the state-of-the-art entropy conserving method and our entropy stable DP SBP method conserve total mass and total absolute vorticity up to rounding errors. While the entropy conserving method conserves total entropy up to machine errors, nevertheless, it sustains total enstrophy growth leading the accumulation of high frequency errors which pollutes the solution. However, our proposed entropy stable DP SBP framework dissipate both total entropy/energy and total enstrophy and keeps the solution stable and accurate.

5.2.4 Barotropic shear instability

Our final numerical example for the nonlinear shallow water equation is the the barotropic shear instability [35, 66, 67]. This is also known as the Kelvin-Helmholtz instability, and involves triggering a barotropic shear within zonal jets by initializing the flow with a thin fluid discontinuity, supplemented with small Gaussian perturbations.

The computational domain is $\Omega = [0, L_x] \times [0, L_y]$, with $L_x = L_y = 4 \times 10^7$ m with doubly periodic boundary conditions.

$$u_0 = \bar{u}_0 \left(\text{sech}(10^{-6}(y - y_+)) - \text{sech}(10^{-6}(y - y_-)) \right), \quad v_0 = 0, \quad h_0 = H - \frac{f}{g} \int_0^y u(x, s) ds + \tilde{h}(x, y), \quad (105)$$

with

$$\tilde{h}(x, y) = \bar{h}_0 \left(e^{-k \times d_1(x, y)} + e^{-k \times d_2(x, y)} \right), \quad d_i(x, y) = \frac{(x - x_i)^2}{L_x^2} + \frac{(y - y_i)^2}{L_y^2}, \quad i = \{1, 2\},$$

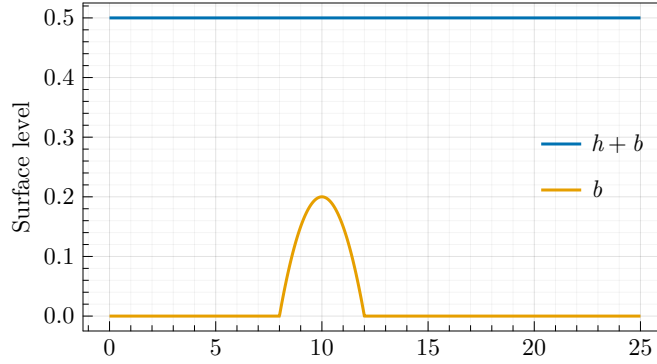
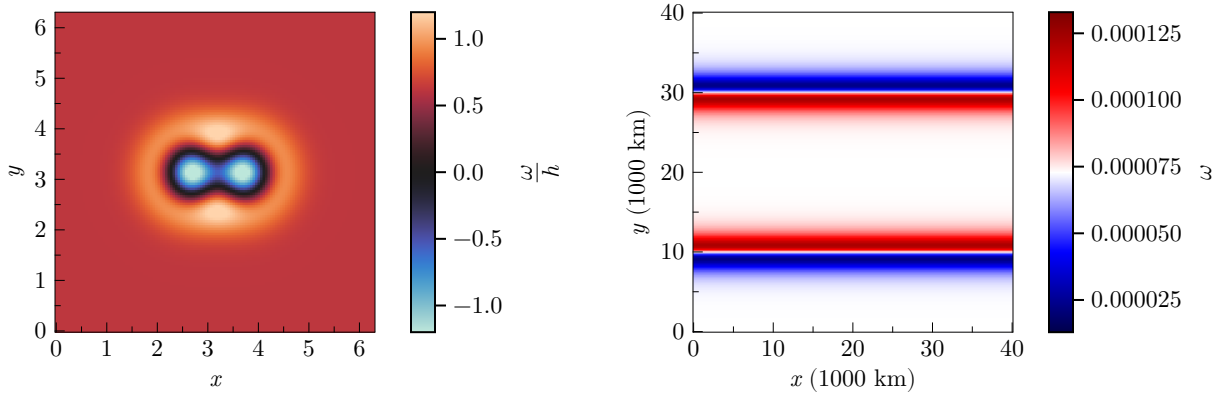


Figure 6: The exact solution for the 1D lake at rest with an immersed bump.



(a) Initial potential vorticity for the merging vortex problem. (b) Initial absolute vorticity for the barotropic shear instability.

Figure 7: Initial conditions for the numerical simulations of the 2D shallow water equations.

where $\bar{h}_0 = 0.01 \times H$, $(x_1, y_1) = (0.85 \times L_x, y_-)$, $(x_2, y_2) = (0.15 \times L_x, y_+)$, and

$$y_+ = 0.25L_y, y_- = 0.75L_y, \bar{u}_0 = 50 \text{ m s}^{-1}, f = 7.292 \times 10^{-5}, g = 9.80616 \text{ m s}^{-2}, H = 10 \text{ km}, k = 10^3.$$

The initial condition for absolute vorticity is plotted in Figure 7b.

We discretise the spatial domain using 256×256 grid points with uniform spatial step $\Delta x = \Delta y > 0$ and evolve the numerical solution until the final time $t = 5 \times 10^6$ s with the time-step $\Delta t = 0.05\Delta x$. The dynamics of the absolute vorticity ω are shown in Figure 8, where we also compare our entropy-stable DP-SBP framework with the state-of-the-art entropy conserving split-form SBP method. Similar to the merging vortices, simulated in the last example, our entropy stable DP-SBP framework remains stable and preserves the structures of the vortices. Meanwhile, the state-of-the-art entropy conserving method generates large amount of numerical noise which destroys the structure of the vortices and could eventually crash the simulation.

5.3 The compressible Euler equations

We consider the compressible Euler equations of gas dynamics in 1D and 2D. The skew-symmetric form and the semi-discrete approximation (in 2D) is briefly discussed in Appendix C. As before, we will perform numerical experiments to verify accuracy and demonstrate robustness. In particular, we will consider the Kelvin Helmholtz instability with fully developed turbulence and demonstrate that our framework provides significant improvements over the state-of-the-art methods.

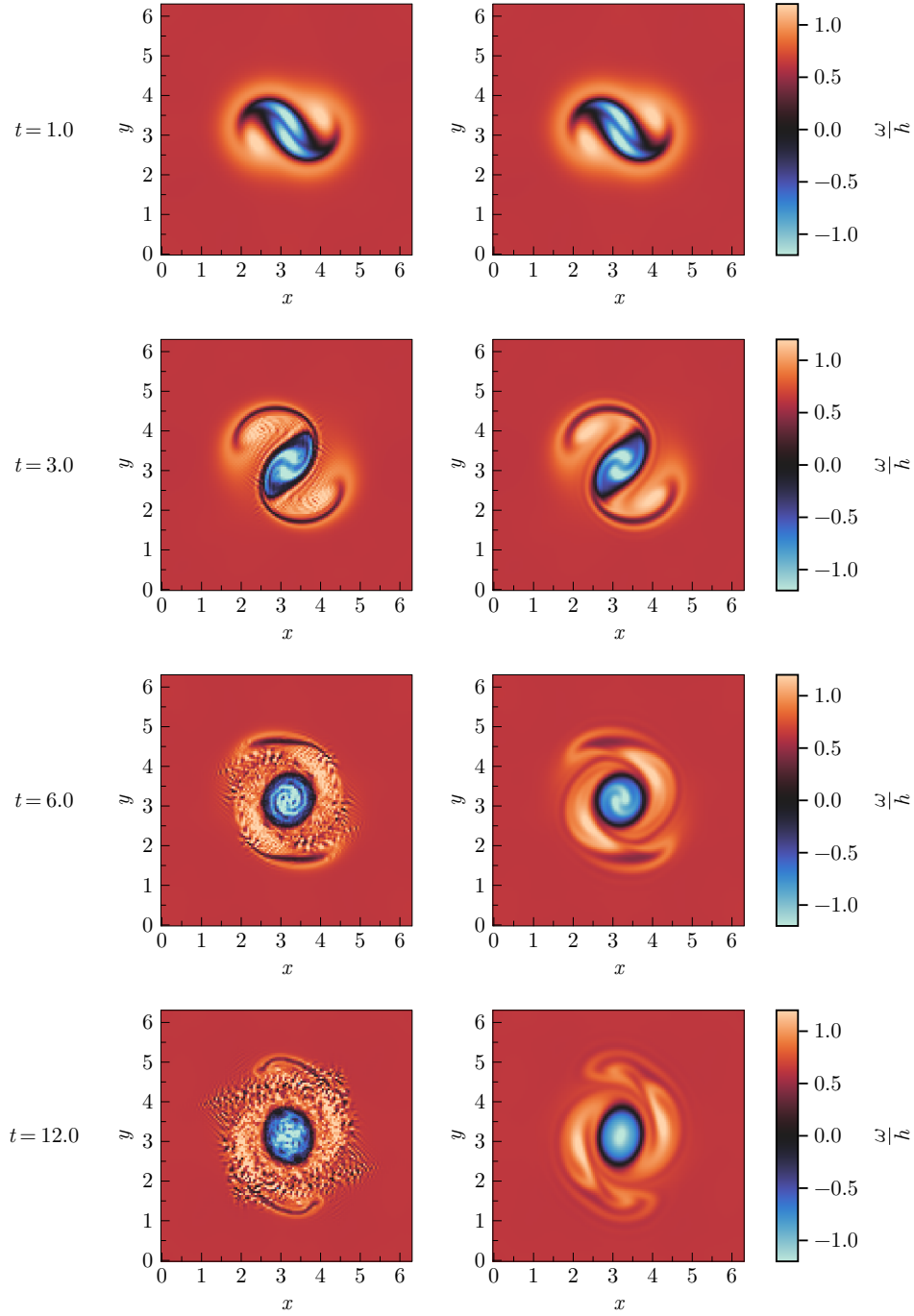


Figure 8: The potential vorticity for the 2D merging vortices problem [35, 65], on a 128×128 grid resolution using 7-th order accurate DP SBP operator, modeled by the nonlinear rotating shallow water equation. The left panel corresponds to the state-of-the-art 7th order accurate entropy conserving split-form SBP method, while the right panel is our proposed 7th order accurate DP-SBP framework. **No artificial viscosity, filtering or limiting was used.** Note that initially ($t \leq 3$) the solutions computed by the two methods look similar, with little numerical artifacts present in the state-of-the-art entropy conserving method. However, later ($t > 3$), while our DP-SBP framework remains stable and preserves the structures of the vortices, the state-of-the-art entropy conserving method generates large numerical oscillations which destroys the structure of the vortices and eventually crashes the simulation.

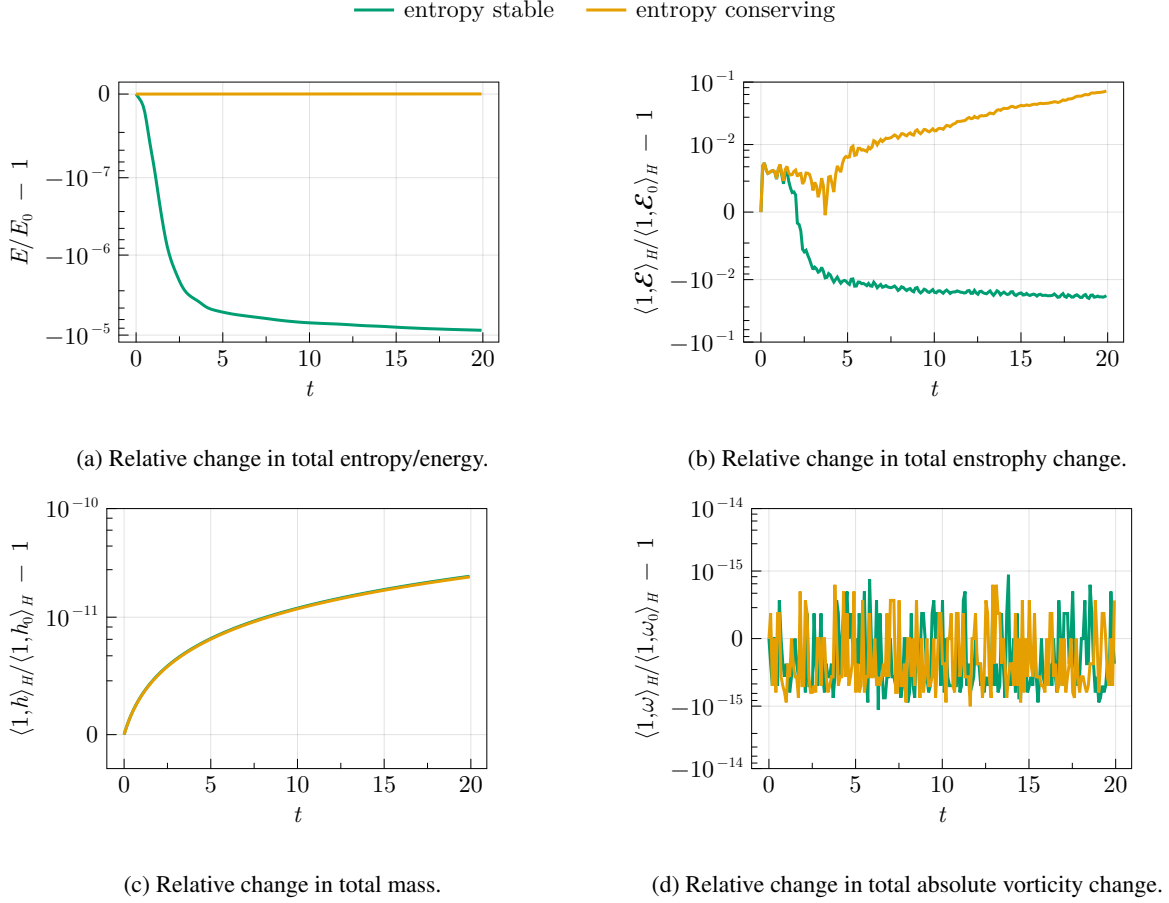


Figure 9: The relative change of the invariants for the merging vortices modeled by the 2D nonlinear shallow water equations.

5.3.1 Convergence tests for the 1D compressible Euler equations

To verify accuracy, we force the 1D compressible Euler equations to satisfy the manufactured (exact) solution

$$\varrho(t, x) = 2 + 0.3 \sin(2\pi(x - t)), \quad u(t, x) = 1, \quad p(t, x) = 2 + 0.3 \sin(2\pi(x + t)), \quad x \in [-1, 1]. \quad (106)$$

We integrate the numerical solution until the final time $t = 2$, on a sequence of increasing mesh resolutions, with the time-step $\Delta t = 0.1 \Delta x$. The rates of convergence, as measured by the l^2 error can be found in Figure 11 and Table 6. Again note that the numerical convergence rates of the errors, recorded in Figure 11 and Table 6, are slightly better than the theoretical rates give in Table 1.

5.3.2 The 2D isentropic vortex problem

To verify numerical accuracy for the 2D compressible Euler equation, we consider the isentropic vortex test problem [69]. Specifically, we use the initial conditions as given by [49]

$$T_0 = \bar{T}_0 - \frac{(\gamma - 1)\varepsilon^2}{8\gamma\pi^2} \exp(1 - r^2), \quad \varrho_0 = \bar{\varrho}_0(T_0/\bar{T}_0)^{1/(\gamma-1)}, \quad \begin{bmatrix} u_0 \\ v_0 \end{bmatrix} = \begin{bmatrix} \bar{u}_0 \\ \bar{v}_0 \end{bmatrix} + \frac{\varepsilon}{2\pi} \exp((1 - r^2)/2) \begin{bmatrix} -y \\ x \end{bmatrix}, \quad p_0 = \bar{T}_0 \bar{\varrho}_0,$$

where $\varepsilon = 10$ is the vortex strength, $r = \sqrt{x^2 + y^2}$, T is the temperature, $\bar{\varrho}_0 = 1$ is the background density, $\bar{u}_0 = \bar{v}_0 = 1$ is the background velocity, $p_0 = 10$ is the background pressure, $\gamma = 1.4$, and $\bar{T}_0 = p_0/\bar{\varrho}_0$ the background temperature, with spatial domain $[-8, 8]^2$ and periodic boundary condition. As shown in Figure 12, the exact solution is the initial vortex translating diagonally along the domain, and because of the periodic boundary conditions re-enters the domain through the corners.

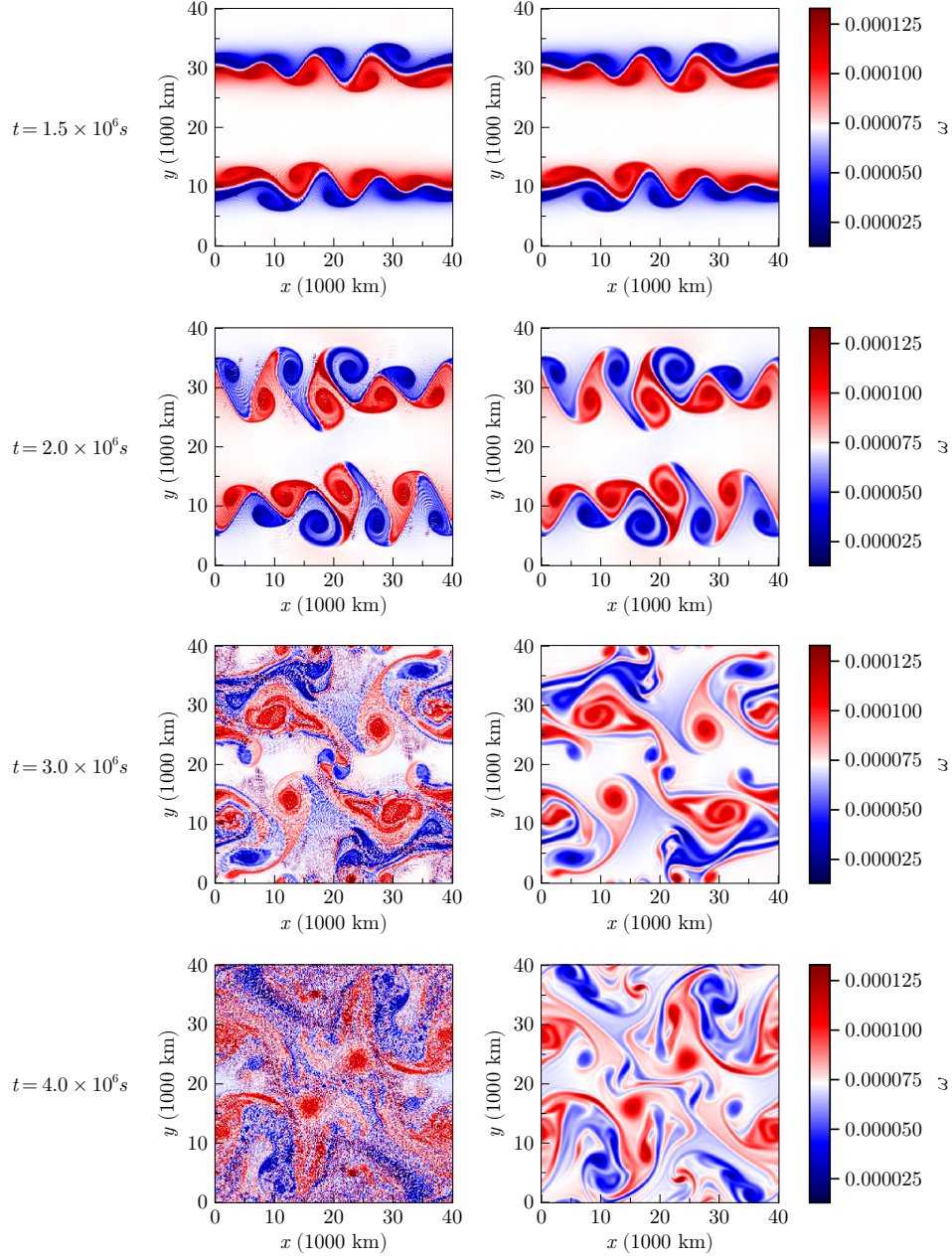


Figure 10: The vorticity dynamics for the barotropic shear instability [35, 66, 67], on a 256×256 grid resolution using 7-th order accurate DP SBP operator, modeled by the nonlinear rotating shallow water equation with fully developed turbulence. The left panel corresponds to the state-of-the-art 7-th order interior accurate entropy conserving split-form SBP method, while the right panel is our proposed 7-th order accurate DP-SBP framework. **No artificial viscosity, filtering or limiting was used.** Note that initially ($t \leq 2 \times 10^6$) the solutions computed by the two methods look similar. However, later ($t > 2 \times 10^6$), while DP-SBP framework remains stable and preserves the structures of the vortices, the state-of-the-art entropy conserving method generates large numerical oscillations which destroys the structure of the vortices and eventually crashes the simulation.

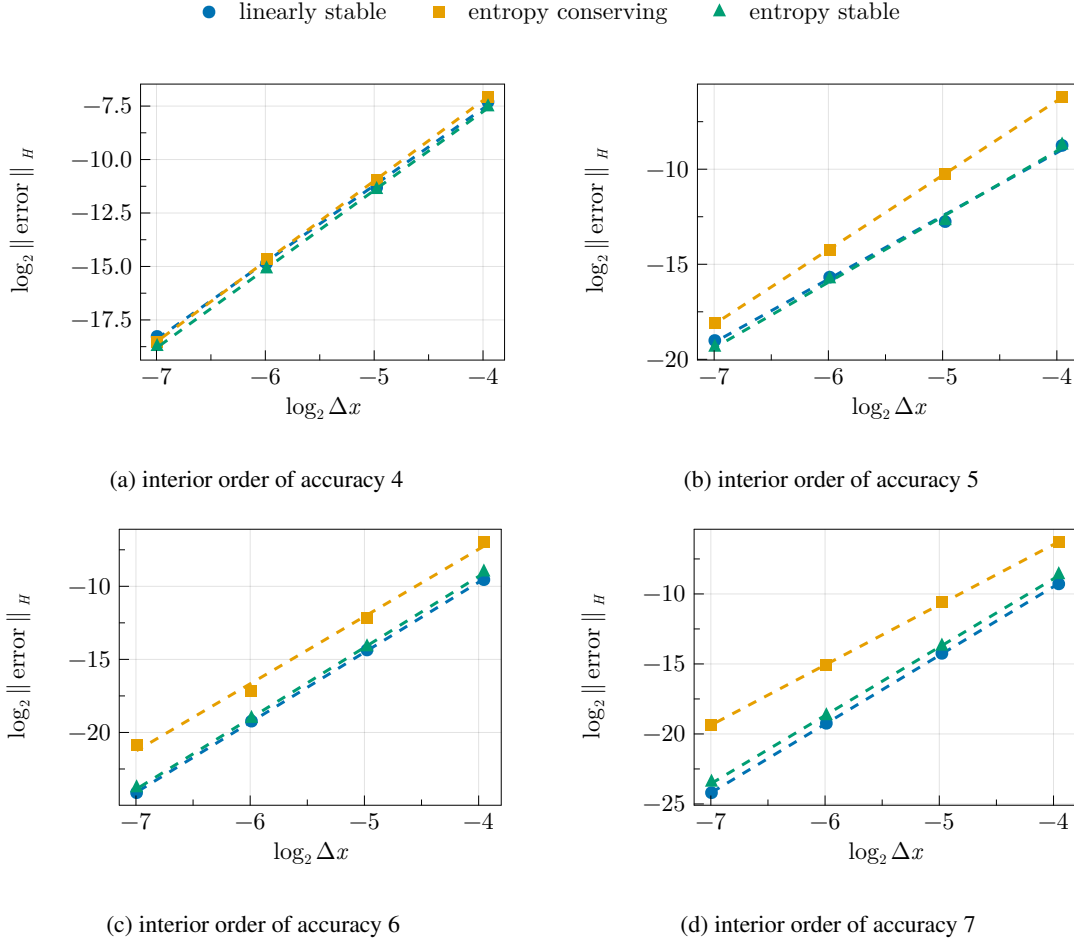


Figure 11: The l^2 numerical errors at $t = 2$ for the 1D compressible Euler equations.

We run the simulation on a sequence of increasing uniform mesh resolutions, $\Delta x = \Delta y > 0$, until the final time $t = 16$, with time-step of $\Delta t = 0.1\Delta x$. The l^2 errors and the convergence rates of the errors are displayed in Figure 13 and Table 7. Similarly, we note that the numerical convergence rates of the errors, shown in Figure 13 and Table 7, are slightly better than the theoretical rates give in Table 1. Note, however, on a coarse mesh with $N = 32$ grid-points in both x - and y -axis the 7-th order accurate and the linearly stable method is numerically unstable. This is an indication of the fragility of linearly stable high order methods when used to solve nonlinear conservation laws.

5.3.3 Two dimensional Kelvin Helmholtz instability

To further investigate the robustness of our entropy-stable numerical framework we simulate the Kelvin-Helmholtz instability for the compressible Euler equations in 2D. The initial conditions are

$$\varrho_0 = \frac{1}{2} + \frac{3}{4}B(x, y), \quad u_0 = \frac{B(x, y) - 1}{2}, \quad v_0 = \frac{\sin(2\pi)}{10}, \quad p_0 = 1, \quad (107)$$

where $B(x, y) = \tanh(15y + 7.5) - \tanh(15y - 7.5)$ and $(x, y) \in [-1, 1]^2$.

We set the final time $t = 10$ and discretize the computational domain $(x, y) \in [-1, 1]^2$ with a sequence of uniform spatial steps $\Delta x = \Delta y > 0$. Following [49], we also formulate linearly stable upwind SBP methods using the global Lax-Friedrichs and Van Leer-Hänel finite volume flux splitting. For all the 4 methods considered, we evolve the numerical solutions until the final time with a time-step $\Delta t = 0.05\Delta x$. In Table 8 we present the end times of the simulations for different methods and mesh resolutions. Note that the numerical simulations with end times $t < 10$ crashed before the set final time $t = 10$. The linearly stable Lax-Friedrichs and Van Leer-Hänel finite

N	linearly stable		entropy conserving		entropy stable		N	linearly stable		entropy conserving		entropy stable	
	Error	EOC	Error	EOC	Error	EOC		Error	EOC	Error	EOC	Error	EOC
32	6.33e-03	-	7.50e-03	-	5.36e-03	-	32	2.32e-03	-	1.38e-02	-	2.34e-03	-
64	3.95e-04	3.91	5.01e-04	3.82	3.68e-04	3.78	64	1.45e-04	3.92	8.16e-04	3.98	1.49e-04	3.89
128	3.40e-05	3.50	3.92e-05	3.63	2.81e-05	3.67	128	1.91e-05	2.89	5.10e-05	3.96	1.78e-05	3.03
256	3.16e-06	3.41	2.62e-06	3.88	2.27e-06	3.61	256	1.90e-06	3.31	3.62e-06	3.80	1.47e-06	3.58

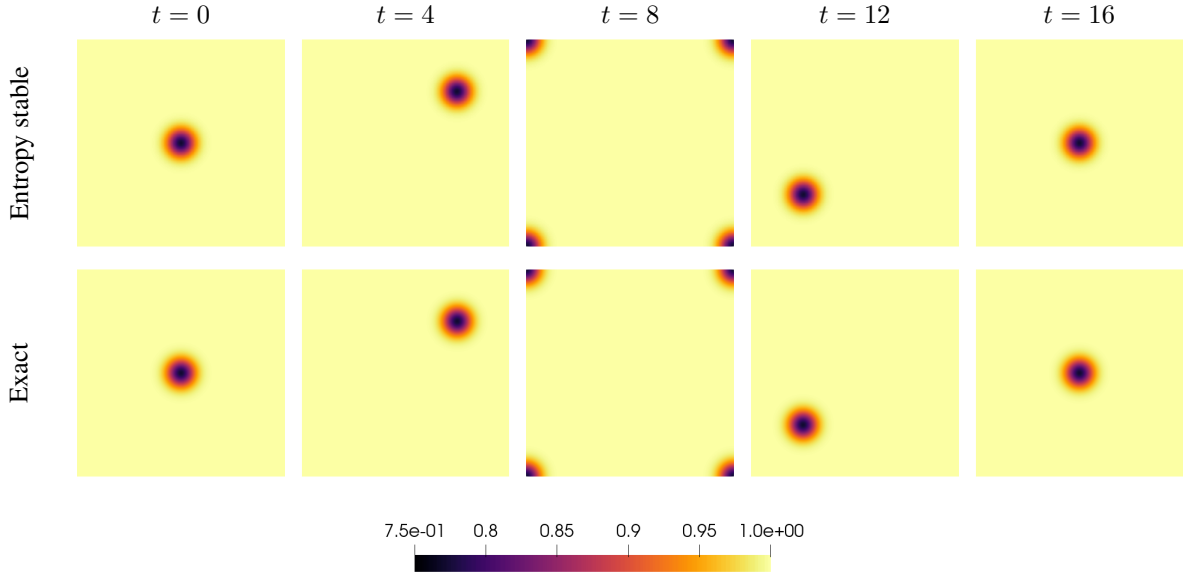
(a) interior order of accuracy 4

N	linearly stable		entropy conserving		entropy stable		N	linearly stable		entropy conserving		entropy stable	
	Error	EOC	Error	EOC	Error	EOC		Error	EOC	Error	EOC	Error	EOC
32	1.34e-03	-	8.07e-03	-	1.91e-03	-	32	1.61e-03	-	1.25e-02	-	2.52e-03	-
64	4.76e-05	4.70	2.19e-04	5.08	5.50e-05	5.00	64	5.15e-05	4.85	6.48e-04	4.18	7.33e-05	4.99
128	1.63e-06	4.82	6.92e-06	4.93	1.84e-06	4.84	128	1.61e-06	4.94	2.91e-05	4.43	2.33e-06	4.92
256	5.47e-08	4.87	5.35e-07	3.67	6.86e-08	4.72	256	5.20e-08	4.93	1.49e-06	4.26	8.68e-08	4.72

(c) interior order of accuracy 6

(b) interior order of accuracy 5

(d) interior order of accuracy 7

Table 6: The convergence of the l^2 numerical errors at $t = 2$ for the 1D compressible Euler equations.Figure 12: Snapshots of the density for the isentropic vortex using 7th order DP SBP operators on a 256×256 grid.

volume flux splitting schemes, and the state-of-the-art entropy conserving schemes crashed before the set final time $t = 10$ for most/all configurations. This is consistent with the recent results presented in [49]. See also Figure 15 where we present the snapshots of the solutions, and record the crash times of the methods using the 7th order interior accurate methods on 512×512 mesh resolution. However, it is significantly noteworthy that for all configurations our entropy-stable scheme is stable and reached the set final time $t = 10$ without crashing.

In Figure 14 we plot the relative change of some of the invariants with time. When stable, note that all methods conserve total mass and total momentum up to rounding errors. The entropy conserving method conserves both total energy and total thermodynamic entropy, and crashes before $t = 4$. The linearly stable Lax-Friedrichs and Van Leer-Hänel finite volume flux splitting schemes conserve total energy and dissipate total thermodynamic entropy, but they also crash before $t = 5.5$. Our entropy-stable DP SBP framework dissipates both total energy and total thermodynamic entropy when the flow becomes fully turbulent and, for all configurations, run to the end of the simulation $t = 10$ without crashing. These are strong demonstrations of the robustness of the proposed numerical framework and shows significant improvements over the current state-of-the-arts methods.

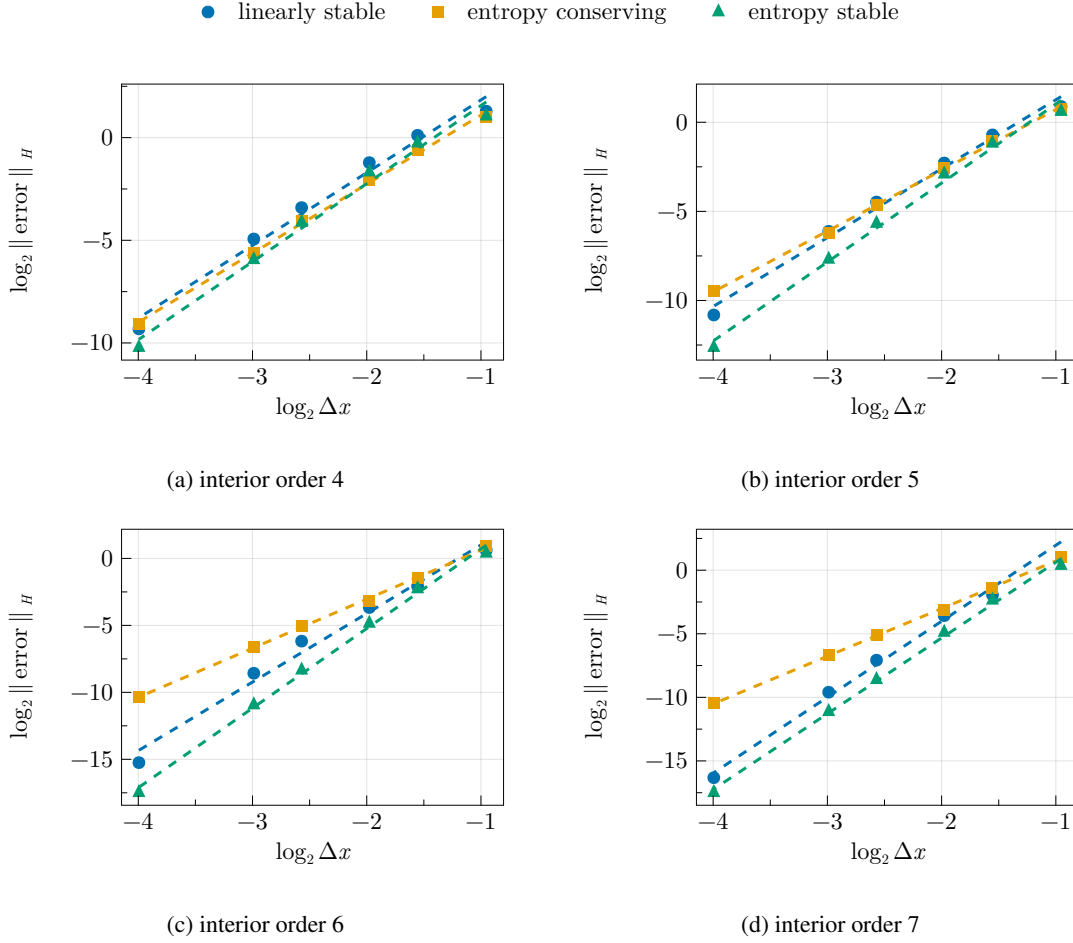


Figure 13: The l^2 numerical errors at $t = 16$ for the 2D the compressible Euler equations.

6 Summary and outlook

The design of provably stable numerical methods for nonlinear hyperbolic conservation laws pose a significant challenge. In this study we have proposed and analyzed the DP and SBP framework for accurate and robust numerical approximations of nonlinear conservation laws. The DP SBP FD operators [47, 48] are a dual-pair of backward and forward difference operators which together preserve the SBP property. In addition, the DP SBP operators are designed to be upwind, that is they come with some built-in dissipation everywhere, as opposed to traditional SBP and DG methods which can only induce dissipation through numerical fluxes acting at element interfaces. We combine the DP SBP operators together with skew-symmetric and upwind flux splitting of nonlinear hyperbolic conservation laws. Our semi-discrete approximation is provably entropy-stable for arbitrary nonlinear hyperbolic conservation laws. Some examples are given to validate the theoretical guarantees, and demonstrate significant improvements over the state-of-the-art methods.

There are multiple directions in which this work can be extended. Important and possible directions for future work include numerical treatments of non-periodic boundary conditions, multi-block schemes and curvilinear meshes to handle complex geometries and 2D manifolds, local energy stability analysis, proper treatments of supersonic shocks, extensions to more complex applications like thermal shallow water equations, moist compressible Euler equations and multi-component compressible Euler equations with chemistry, and to other PDEs such as magnetohydrodynamics equations and plasma simulations.

N	linearly stable		entropy conserving		entropy stable		N	linearly stable		entropy conserving		entropy stable	
	Error	EOC	Error	EOC	Error	EOC		Error	EOC	Error	EOC	Error	EOC
32	2.44e+00	-	1.98e+00	-	2.07e+00	-	32	1.85e+00	-	1.69e+00	-	1.52e+00	-
48	1.08e+00	1.96	6.63e-01	2.63	8.31e-01	2.19	48	6.12e-01	2.65	4.90e-01	2.98	4.41e-01	2.97
64	4.30e-01	3.14	2.42e-01	3.44	3.13e-01	3.34	64	2.05e-01	3.73	1.66e-01	3.69	1.33e-01	4.10
96	9.43e-02	3.70	5.90e-02	3.44	5.72e-02	4.13	96	4.50e-02	3.70	4.07e-02	3.43	1.95e-02	4.67
128	3.27e-02	3.65	2.01e-02	3.71	1.62e-02	4.35	128	1.44e-02	3.93	1.36e-02	3.77	4.84e-03	4.81
256	1.57e-03	4.35	1.85e-03	3.42	8.36e-04	4.25	256	5.56e-04	4.67	1.42e-03	3.25	1.57e-04	4.92

(a) 4th order interior accurate

N	linearly stable		entropy conserving		entropy stable		N	linearly stable		entropy conserving		entropy stable	
	Error	EOC	Error	EOC	Error	EOC		Error	EOC	Error	EOC	Error	EOC
32	1.53e+00	-	1.89e+00	-	1.31e+00	-	32	NaN	-	2.04e+00	-	1.29e+00	-
48	2.38e-01	4.47	3.55e-01	4.02	2.06e-01	4.44	48	2.60e-01	NaN	3.72e-01	4.08	1.95e-01	4.55
64	7.87e-02	3.78	1.12e-01	3.94	3.47e-02	6.08	64	8.39e-02	3.86	1.16e-01	3.99	3.36e-02	6.00
96	1.38e-02	4.23	3.04e-02	3.17	3.07e-03	5.90	96	7.42e-03	5.91	2.98e-02	3.31	2.56e-03	6.27
128	2.63e-03	5.72	1.03e-02	3.73	5.08e-04	6.20	128	1.29e-03	6.02	9.68e-03	3.87	4.47e-04	6.01
256	2.57e-05	6.64	7.62e-04	3.74	5.42e-06	6.51	256	1.22e-05	6.69	6.99e-04	3.77	5.39e-06	6.34

(c) 6th order interior accurate

(b) 5th order interior accurate

(d) 7th order interior accurate

Table 7: The convergence of the l^2 numerical errors at $t = 16$ for the 2D compressible Euler equations.

N	order of accuracy p				N	order of accuracy p			
	4	5	6	7		4	5	6	7
64	10	10	4.34	4.07	64	10	5.22	4.57	4.56
128	4.23	4.33	4.59	4.56	128	10	10	4.68	4.69
256	10	10	5.74	4.54	256	10	10	4.77	4.72
512	10	10	5.54	5.70	512	10	10	4.82	4.64

(a) linearly stable

N	order of accuracy p				N	order of accuracy p			
	4	5	6	7		4	5	6	7
64	4.01	3.49	4.09	3.72	64	10	10	10	10
128	4.33	4.76	3.97	4.50	128	10	10	10	10
256	4.25	3.75	4.26	4.26	256	10	10	10	10
512	3.81	3.78	3.93	3.85	512	10	10	10	10

(c) entropy conserving

(b) Van Leer-Hänel

(d) entropy stable

Table 8: The end (crash) times of the numerical simulations of the Kelvin-Helmholtz instability for the compressible Euler equations for different schemes on $N \times N$ grid resolution using $p = 4, 5, 6, 7$ order accurate DP SBP operators. The state-of-the-art entropy conserving method and the linearly stable Lax-Friedrichs and Van Leer-Hänel finite volume flux splitting schemes crashed before the set final time $t = 10$ for most/all configurations. For all configurations our entropy-stable DP SBP scheme is stable and reached the set final time $t = 10$ without crashing.

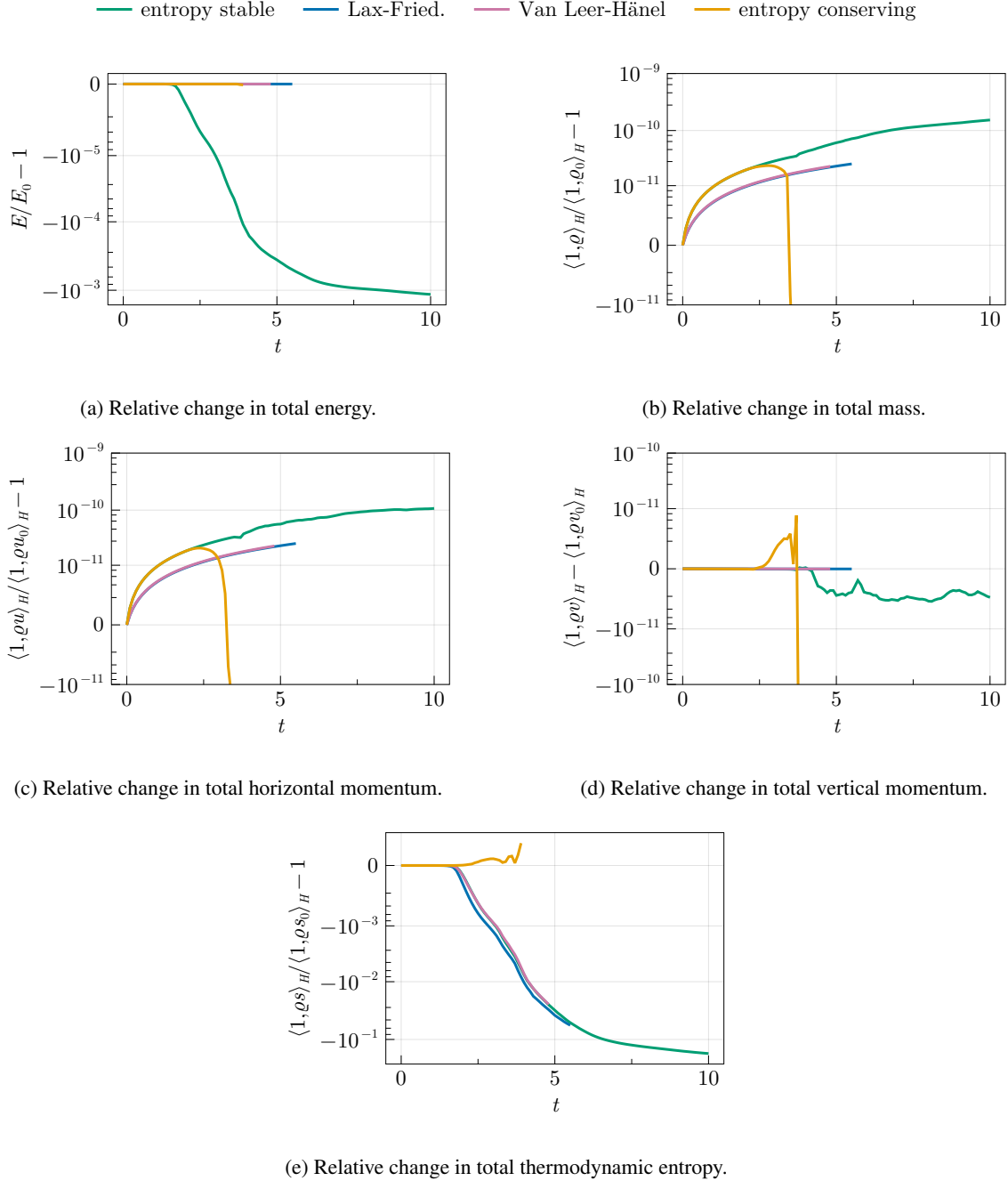


Figure 14: The relative change of the invariants for the 2D Kelvin-Helmholtz instability on 512×512 grid resolution using 7-th order accurate DP SBP operator. Note that $t = 3.9, 4.8, 5.5$ are the crash times of the state-of-the-art entropy conserving method, and the linearly stable upwind SBP methods [49] derived using the global Lax-Friedrichs and Van Leer-Hänel finite volume flux splitting. Our entropy-stable scheme remains stable throughout the simulation $t \in [0, 10]$.

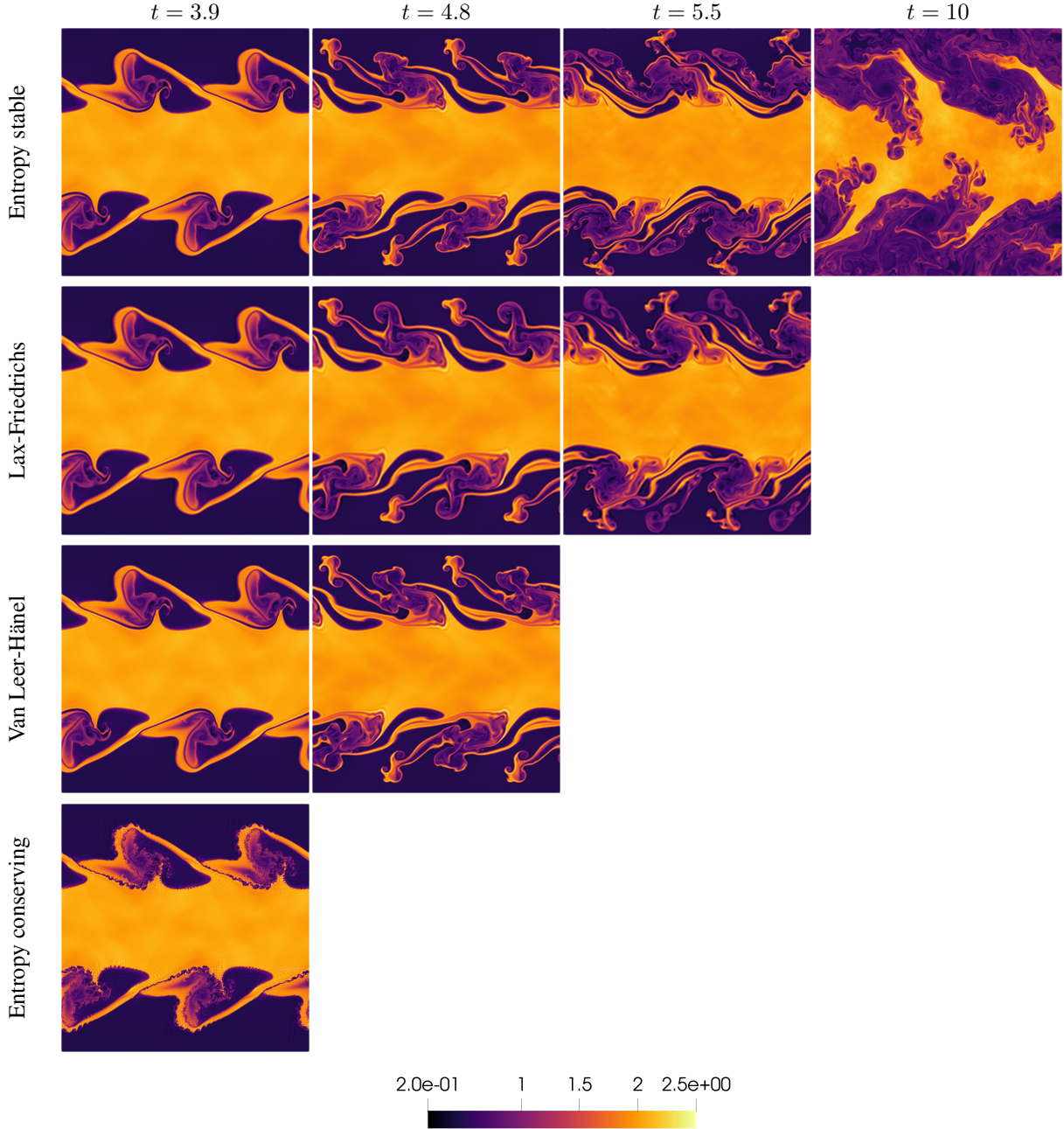


Figure 15: The snapshots of the density for the Kelvin Helmholtz instability modeled by the 2D compressible Euler equation on 512×512 grid resolution using 7-th order accurate DP SBP operator. **No artificial viscosity, filtering or limiting was used.** When stable there seems to be a good agreement between the methods. The snapshots are given at $t = 3.9, 4.8, 5.5$, and at final time 10. Note that $t = 3.9, 4.8, 5.5$ are the crash times of the state-of-the-art entropy conserving method, and the linearly stable upwind SBP methods [49] derived using the global Lax-Friedrichs and Van Leer-Hänel finite volume flux splitting. Our entropy-stable scheme remains stable throughout the simulation $t \in [0, 10]$. This is a strong demonstration of the robustness of the proposed numerical framework.

A 2D Shallow Water Equations—Flux Form

The 2D shallow water equations in flux form are given by

$$\partial_t h + \nabla \cdot (h\mathbf{u}) = 0, \quad (108)$$

$$\partial_t(hu) + \partial_x \left(hu^2 + \frac{1}{2}gh^2 \right) + \partial_y(huv) = 0, \quad (109)$$

$$\partial_t(hv) + \partial_y \left(hv^2 + \frac{1}{2}gh^2 \right) + \partial_x(huv) = 0, \quad (110)$$

where $\mathbf{u} = [u, v]^\top$ is the fluid velocity, $h > 0$ is the height of the fluid, and $g > 0$ is the gravitational acceleration.

The skew symmetric form is given by

$$\partial_t h + \nabla \cdot (h\mathbf{u}) = 0, \quad (111)$$

$$\partial_t(hu) + \frac{1}{2}(\partial_x hu^2 + u\partial_x hu + hu\partial_x u) + gh\partial_x h + \frac{1}{2}(\partial_y huv + u\partial_y hv + hv\partial_y u) = 0, \quad (112)$$

$$\partial_t(hv) + \frac{1}{2}(\partial_y hv^2 + v\partial_y hv + hv\partial_y v) + gh\partial_y h + \frac{1}{2}(\partial_x huv + u\partial_x hv + hv\partial_x u) = 0. \quad (113)$$

For $\mathbf{U} = (h, hu, hv)^T$ and $e = \frac{1}{2}h(u^2 + v^2) + \frac{1}{2}gh^2 = \frac{1}{2h}((hu)^2 + (hv)^2) + \frac{1}{2}gh^2$ we have

$$\mathbf{q} = h\mathbf{u} \left(\frac{1}{2}|\mathbf{u}|^2 + gh \right), \quad \mathbf{g} = \begin{bmatrix} gh - |\mathbf{u}|^2 \\ u \\ v \end{bmatrix}$$

$$\mathbf{F}(\mathbf{U}, \mathbf{f}(\mathbf{U}), \partial_{\mathbf{x}}) := \begin{bmatrix} \nabla \cdot (h\mathbf{u}) \\ \frac{1}{2}(\partial_x hu^2 + u\partial_x hu + hu\partial_x u) + gh\partial_x h + \frac{1}{2}(\partial_y huv + u\partial_y hv + hv\partial_y u) \\ \frac{1}{2}(\partial_y hv^2 + v\partial_y hv + hv\partial_y v) + gh\partial_y h + \frac{1}{2}(\partial_x huv + u\partial_x hv + hv\partial_x u) \end{bmatrix}$$

Using only integration by parts and some algebraic manipulations it is straightforward to show that (32) hold, that is

$$(\mathbf{g}, \mathbf{F}(\mathbf{U}, \mathbf{f}(\mathbf{U}), \partial_{\mathbf{x}})) = (1, \nabla \cdot \mathbf{q}) = \oint_{\partial\Omega} (\mathbf{q} \cdot \mathbf{n}) d\mathbf{x}, \quad (114)$$

thus leading to

$$\partial_t E + \oint_{\partial\Omega} (\mathbf{q} \cdot \mathbf{n}) d\mathbf{x} = 0.$$

Using the Kronecker product \otimes , the 2D DP derivative operators are defined as $\mathbf{D}_{\pm x} = D_{\pm} \otimes \mathbf{I}_y$, $\mathbf{D}_{\pm y} = \mathbf{I}_x \otimes D_{\pm}$ where D_{\pm} are 1D DP operators closed with penalty periodic boundary, and satisfy $D_+ + D_-^T = 0$. The 2D SBP norm is defined as $\mathbf{H} = (H \otimes H)$ and $\mathbf{I}_x, \mathbf{I}_y \in \mathbb{R}^{N \times N}$ being identity matrices. The entropy stable semi-discrete approximation reads

$$\partial_t \mathbf{U} + \mathbf{F}(\mathbf{U}, \mathbf{f}(\mathbf{U}), \mathbf{D}) = \sum_{\eta=x,y} (\Gamma_{\eta} \otimes \mathcal{D}_{\eta}) \mathbf{g}, \quad \mathbf{D} = (\mathbf{D}_x, \mathbf{D}_y), \quad \mathcal{D}_{\eta} = \frac{1}{2}(\mathbf{D}_{\eta+} - \mathbf{D}_{\eta-}) \quad (115)$$

where $c = |\mathbf{u}| + \sqrt{gh}$ and

$$\Gamma_x = \text{diag} \left(\left[2 \max_{x,y} \frac{h}{c}, 4 \max_{x,y} \left(h \left(c - \frac{1}{2} \sqrt{gh} \right) \right), 4 \max_{x,y} h \sqrt{|uv|} \right] \right)$$

$$\Gamma_y = \text{diag} \left(\left[2 \max_{x,y} \frac{h}{c}, 4 \max_{x,y} h \sqrt{|uv|}, 4 \max_{x,y} \left(h \left(c - \frac{1}{2} \sqrt{gh} \right) \right) \right] \right).$$

B Shallow Water Equations—Vector-Invariant Form

The vector-invariant shallow water equations on a flat plane are given by

$$\partial_t h + \nabla \cdot (h\mathbf{u}) = 0 \quad (116a)$$

$$\partial_t u - \omega v + \partial_x G = 0 \quad (116b)$$

$$\partial_t v + \omega u + \partial_y G = 0 \quad (116c)$$

with

$$\omega = \partial_x v - \partial_y u + f \quad G = \frac{1}{2}(u^2 + v^2) + gh,$$

where $\mathbf{u} = [u, v]^\top$ is the fluid velocity, $h > 0$ is the height of the fluid, and $g > 0$ is the gravitational acceleration. The vector invariant form of the shallow water equations is already skew-symmetric.

So we consider $\mathbf{U} = (h, u, v)^\top$ and $e = \frac{1}{2}h(u^2 + v^2) + \frac{1}{2}gh^2$, we have

$$\mathbf{q} = h\mathbf{u} \left(\frac{1}{2}|\mathbf{u}|^2 + gh \right), \quad \mathbf{g} = \begin{bmatrix} G \\ u \\ v \end{bmatrix}, \quad \mathbf{F}(\mathbf{U}, \mathbf{f}(\mathbf{U}), \partial_{\mathbf{x}}) := \begin{bmatrix} \nabla \cdot (h\mathbf{u}) \\ \partial_x G - \omega v \\ \partial_y G + \omega u \end{bmatrix}.$$

Again, using only integration by parts and some algebraic manipulations it is straightforward to show that (32) hold, that is

$$(\mathbf{g}, \mathbf{F}(\mathbf{U}, \mathbf{f}(\mathbf{U}), \partial_{\mathbf{x}})) = (1, \nabla \cdot \mathbf{q}) = \oint_{\partial\Omega} (\mathbf{q} \cdot \mathbf{n}) d\mathbf{x}. \quad (117)$$

We also have

$$\partial_t E + \oint_{\partial\Omega} (\mathbf{q} \cdot \mathbf{n}) d\mathbf{x} = 0.$$

C 2D Compressible Euler Equations for an Ideal Gas

The 2D compressible Euler equations for an ideal gas in conservative form is

$$\partial_t \varrho + \nabla \cdot (\varrho \mathbf{u}) = 0, \quad (118a)$$

$$\partial_t (\varrho \mathbf{u}) + \nabla \cdot (\varrho \mathbf{u} \otimes \mathbf{u} + p\mathbf{I}) = 0, \quad (118b)$$

$$\partial_t e + \nabla \cdot ((e + p)\mathbf{u}) = 0, \quad (118c)$$

$$\frac{p}{\gamma - 1} + \frac{1}{2}\varrho(u^2 + v^2) = e. \quad (118d)$$

Here ϱ is the density of the fluid, $\mathbf{u} = [u, v]^\top$ is the velocity, p is the pressure, $\gamma > 1$ is the ratio of specific heats, and e is the energy density. We can see that the energy density e satisfies a conservation law and the total energy $E(t) = \int_{\Omega} e d\mathbf{x}$ is conserved.

The skew-symmetric form derived by Nordström in [30] is

$$2\partial_t \sqrt{\varrho} + \mathbf{u} \cdot \nabla \sqrt{\varrho} + \nabla \cdot \mathbf{u} \sqrt{\varrho} = 0 \quad (119a)$$

$$2\partial_t \sqrt{\varrho} u + \mathbf{u} \cdot \nabla \sqrt{\varrho} u + \nabla \cdot \mathbf{u} \sqrt{\varrho} u + 4 \frac{\sqrt{p}}{\sqrt{\varrho}} \partial_x \sqrt{p} = 0 \quad (119b)$$

$$2\partial_t \sqrt{\varrho} v + \mathbf{u} \cdot \nabla \sqrt{\varrho} v + \nabla \cdot \mathbf{u} \sqrt{\varrho} v + 4 \frac{\sqrt{p}}{\sqrt{\varrho}} \partial_y \sqrt{p} = 0 \quad (119c)$$

$$2\partial_t \sqrt{p} + \gamma \nabla \cdot \mathbf{u} \sqrt{p} + (2 - \gamma) \mathbf{u} \cdot \nabla \sqrt{p} = 0 \quad (119d)$$

with the entropy density e given by

$$e := (\sqrt{\varrho})^2 + \frac{1}{2}(\sqrt{\varrho} u)^2 + \frac{1}{2}(\sqrt{\varrho} v)^2 + \frac{1}{\gamma - 1}(\sqrt{p})^2. \quad (120)$$

If we introduce $\mathbf{U} = (\sqrt{\varrho}, \sqrt{\varrho} u, \sqrt{\varrho} v, \sqrt{p})^\top$ then we have

$$\mathbf{g} = \begin{bmatrix} 2\sqrt{\varrho} \\ \sqrt{\varrho} u \\ \sqrt{\varrho} v \\ \frac{2}{\gamma - 1} \sqrt{p} \end{bmatrix}, \quad \mathbf{q} = \left((\sqrt{\varrho})^2 + \frac{1}{2}(\sqrt{\varrho} u)^2 + \frac{1}{2}(\sqrt{\varrho} v)^2 + \frac{\gamma}{\gamma - 1}(\sqrt{p})^2 \right) \mathbf{u},$$

$$\mathbf{F}(\mathbf{U}, \mathbf{f}(\mathbf{U}), \partial_{\mathbf{x}}) := \frac{1}{2} \begin{bmatrix} \mathbf{u} \cdot \nabla \sqrt{\varrho} + \nabla \cdot \mathbf{u} \sqrt{\varrho} \\ \mathbf{u} \cdot \nabla \sqrt{\varrho} u + \nabla \cdot \mathbf{u} \sqrt{\varrho} u + 4 \frac{\sqrt{p}}{\sqrt{\varrho}} \partial_x \sqrt{p} \\ \mathbf{u} \cdot \nabla \sqrt{\varrho} v + \nabla \cdot \mathbf{u} \sqrt{\varrho} v + 4 \frac{\sqrt{p}}{\sqrt{\varrho}} \partial_y \sqrt{p} \\ \gamma \nabla \cdot \mathbf{u} \sqrt{p} + (2 - \gamma) \mathbf{u} \cdot \nabla \sqrt{p} \end{bmatrix}.$$

As above, using only integration by parts and some algebraic manipulations it is straightforward to show that (32) hold, that is

$$(\mathbf{g}, \mathbf{F}(\mathbf{U}, \mathbf{f}(\mathbf{U}), \partial_{\mathbf{x}})) = (1, \nabla \cdot \mathbf{q}) = \oint_{\partial\Omega} (\mathbf{q} \cdot \mathbf{n}) d\mathbf{x}. \quad (121)$$

We also have

$$\partial_t E + \oint_{\partial\Omega} (\mathbf{q} \cdot \mathbf{n}) d\mathbf{x} = 0.$$

The entropy stable and conservative semi-discrete approximation of the compressible Euler equations in 2D is given by

$$\partial_t \mathbf{U} + \mathbf{F}(\mathbf{U}, \mathbf{f}(\mathbf{U}), \mathbf{D}) = \sum_{\eta=x,y} S_{\eta}(\Gamma_{\eta}, \mathbf{U}, \mathcal{D}_{\eta}), \quad \mathbf{D} = (\mathbf{D}_x, \mathbf{D}_y), \quad \mathcal{D}_{\eta} = \frac{1}{2}(\mathbf{D}_{\eta-} - \mathbf{D}_{\eta+}),$$

where $\Gamma_{\eta} = \text{diag}([\gamma_{\eta 1}, \gamma_{\eta 2}, \gamma_{\eta 3}])$ and

$$S_{\eta}(\Gamma_{\eta}, \mathbf{U}, \mathcal{D}_{\eta}) = \frac{\gamma_{\eta 1}}{\sqrt{\varrho}} \begin{bmatrix} \mathcal{D}_{\eta} \sqrt{\varrho} \\ \mathcal{D}_{\eta} \left(\sqrt{\varrho} u \right) \\ \mathcal{D}_{\eta} \left(\sqrt{\varrho} v \right) \\ 0 \end{bmatrix} + \left(\frac{\gamma_{\eta 2}}{\sqrt{\varrho}} - \gamma_{\eta 1} \right) \begin{bmatrix} 0 \\ \mathcal{D}_{\eta} \mathbf{u} \\ \mathcal{D}_{\eta} \mathbf{v} \\ 0 \end{bmatrix} + \gamma_{\eta 3} \begin{bmatrix} 0 \\ 0 \\ 0 \\ \mathcal{D}_{\eta} p \end{bmatrix}, \quad (122)$$

$$\gamma_{x1} = \frac{1}{4} \max \sqrt{\varrho} \left(|u| + \sqrt{\gamma \frac{p}{\varrho}} \right), \quad \gamma_{x2} = \frac{1}{2} \max \varrho \left(|u| + \sqrt{\gamma \frac{p}{\varrho}} \right), \quad \gamma_{x3} = \frac{1}{2} \max \left(|u| + \sqrt{\gamma \frac{p}{\varrho}} \right), \quad (123)$$

$$\gamma_{y1} = \frac{1}{4} \max \sqrt{\varrho} \left(|v| + \sqrt{\gamma \frac{p}{\varrho}} \right), \quad \gamma_{y2} = \frac{1}{2} \max \varrho \left(|v| + \sqrt{\gamma \frac{p}{\varrho}} \right), \quad \gamma_{y3} = \frac{1}{2} \max \left(|v| + \sqrt{\gamma \frac{p}{\varrho}} \right). \quad (124)$$

References

- [1] J. VonNeumann and R. D. Richtmyer. A Method for the Numerical Calculation of Hydrodynamic Shocks. *Journal of Applied Physics*, 21(3):232–237, 03 1950.
- [2] Peter D. Lax. Weak solutions of nonlinear hyperbolic equations and their numerical computation. *Communications on Pure and Applied Mathematics*, 7(1):159–193, 1954.
- [3] Peter Lax and Burton Wendroff. Systems of conservation laws. *Communications on Pure and Applied Mathematics*, 13(2):217–237, 1960.
- [4] Sergei K. Godunov and I. Bohachevsky. Finite difference method for numerical computation of discontinuous solutions of the equations of fluid dynamics. *Matematicheskij sbornik*, 47(89)(3):271–306, 1959.
- [5] Amiram Harten. On the symmetric form of systems of conservation laws with entropy. *Journal of Computational Physics*, 49(1):151–164, 1983.
- [6] Björn Sjögreen and H. C. Yee. Entropy stable method for the euler equations revisited: Central differencing via entropy splitting and sbp. *Journal of Scientific Computing*, 81(3):1359–1385, 2019.
- [7] Margot Gerritsen and Pelle Olsson. Designing an efficient solution strategy for fluid flows: 1. a stable high order finite difference scheme and sharp shock resolution for the euler equations. *Journal of Computational Physics*, 129(2):245–262, 1996.
- [8] Travis C. Fisher, Mark H. Carpenter, Jan Nordström, Nail K. Yamaleev, and Charles Swanson. Discretely conservative finite-difference formulations for nonlinear conservation laws in split form: Theory and boundary conditions. *Journal of Computational Physics*, 234:353–375, 2013.
- [9] Vidar Stiernström, Lukas Lundgren, Murtazo Nazarov, and Ken Mattsson. A residual-based artificial viscosity finite difference method for scalar conservation laws. *Journal of Computational Physics*, 430:110100, 2021.
- [10] Jan Nordström. Conservative finite difference formulations, variable coefficients, energy estimates and artificial dissipation. *Journal of Scientific Computing*, 29(3):375–404, 2006.
- [11] Ken Mattsson, Magnus Svärd, and Jan Nordström. Stable and accurate artificial dissipation. *Journal of Scientific Computing*, 21(1):57–79, 2004.
- [12] Ann E. Mattsson and W. J. Rider. Artificial viscosity: back to the basics. *International Journal for Numerical Methods in Fluids*, 77(7):400–417, 2015.

- [13] Mark H. Carpenter, Travis C. Fisher, Eric J. Nielsen, and Steven H. Frankel. Entropy stable spectral collocation schemes for the navier–stokes equations: Discontinuous interfaces. *SIAM Journal on Scientific Computing*, 36(5):B835–B867, 2014.
- [14] Gregor J. Gassner, Andrew R. Winters, and David A. Kopriva. Split form nodal discontinuous galerkin schemes with summation-by-parts property for the compressible euler equations. *Journal of Computational Physics*, 327:39–66, 2016.
- [15] Gregor J. Gassner, Andrew R. Winters, and David A. Kopriva. A well balanced and entropy conservative discontinuous galerkin spectral element method for the shallow water equations. *Applied Mathematics and Computation*, 272:291–308, 2016. Recent Advances in Numerical Methods for Hyperbolic Partial Differential Equations.
- [16] Jesse Chan. On discretely entropy conservative and entropy stable discontinuous galerkin methods. *Journal of Computational Physics*, 362:346–374, 2018.
- [17] G. J. Gassner and A. R. Winters. A novel robust strategy for discontinuous galerkin methods in computational fluid mechanics: Why? when? what? where? *Frontiers in Physics*, 8, 2021.
- [18] Hendrik Ranocha. Comparison of some entropy conservative numerical fluxes for the euler equations. *Journal of Scientific Computing*, 76:216–242, 2018.
- [19] F.X. Giraldo, J.S. Hesthaven, and T. Warburton. Nodal high-order discontinuous galerkin methods for the spherical shallow water equations. *Journal of Computational Physics*, 181(2):499–525, 2002.
- [20] Jesse Chan, Hendrik Ranocha, Andrés M. Rueda-Ramírez, Gregor Gassner, and Tim Warburton. On the entropy projection and the robustness of high order entropy stable discontinuous galerkin schemes for under-resolved flows. *Frontiers in Physics*, 10, 2022.
- [21] Randall J. LeVeque. *Scalar Conservation Laws*, pages 19–40. Birkhäuser Basel, Basel, 1992.
- [22] Randall J. LeVeque. *Finite Volume Methods for Hyperbolic Problems*. Cambridge Texts in Applied Mathematics. Cambridge University Press, 2002.
- [23] Heinz-Otto Kreiss and Joseph Oliger. Comparison of accurate methods for the integration of hyperbolic equations. *Tellus A: Dynamic Meteorology and Oceanography*, Jan 1972.
- [24] Heinz-Otto Kreiss. Initial boundary value problems for hyperbolic systems. *Communications on Pure and Applied Mathematics*, 23(3):277–298, 1970.
- [25] Heinz-Otto Kreiss and Jens Lorenz. *Initial-boundary value problems and the Navier-Stokes equations*. SIAM, 2004.
- [26] Bertil Gustafsson and Arne Sundström. Incompletely parabolic problems in fluid dynamics. *SIAM Journal on Applied Mathematics*, 35(2):343–357, 1978.
- [27] Joseph Oliger and Arne Sundström. Theoretical and practical aspects of some initial boundary value problems in fluid dynamics. *SIAM Journal on Applied Mathematics*, 35(3):419–446, 1978.
- [28] Eitan Tadmor. Entropy stability theory for difference approximations of nonlinear conservation laws and related time-dependent problems. *Acta Numerica*, 12:451–512, 2003.
- [29] Gregor J Gassner, Magnus Svärd, and Florian J Hindenlang. Stability issues of entropy-stable and/or split-form high-order schemes: Analysis of linear stability. *Journal of Scientific Computing*, 90:1–36, 2022.
- [30] Jan Nordström. A skew-symmetric energy and entropy stable formulation of the compressible euler equations. *Journal of Computational Physics*, 470:111573, December 2022.
- [31] Jan Nordström and Fredrik Laurén. The spatial operator in the incompressible navier–stokes, oseen and stokes equations. *Computer Methods in Applied Mechanics and Engineering*, 363:112857, 2020.
- [32] Jan Nordström and Andrew R Winters. A linear and nonlinear analysis of the shallow water equations and its impact on boundary conditions. *Journal of Computational Physics*, 463:111254, 2022.
- [33] Jesse Chan, Hendrik Ranocha, Andres Rueda-Ramirez, Gregor Gassner, and Tim Warburton. On the entropy projection and the robustness of high order entropy stable discontinuous galerkin schemes for under-resolved flows, 2022.
- [34] Kieran Ricardo, Dave Lee, and Kenneth Duru. Conservation and stability in a discontinuous galerkin method for the vector invariant spherical shallow water equations. *Journal of Computational Physics*, 500:112763, 2024.
- [35] Justin Kin Jun Hew, Kenneth Duru, Stephen Roberts, Christopher Zoppou, and Kieran Ricardo. Strongly stable dual-pairing summation by parts finite difference schemes for the vector invariant nonlinear shallow water equations – i: Numerical scheme and validation on the plane, 2024.

- [36] Constantine M Dafermos. The entropy rate admissibility criterion for solutions of hyperbolic conservation laws. *Journal of Differential Equations*, 14(2):202–212, 1973.
- [37] Peter D. Lax. *Hyperbolic Systems of Conservation Laws and the Mathematical Theory of Shock Waves*. Society for Industrial and Applied Mathematics, 1973.
- [38] H-O Kreiss and Godela Scherer. Finite element and finite difference methods for hyperbolic partial differential equations. In *Mathematical aspects of finite elements in partial differential equations*, pages 195–212. Elsevier, 1974.
- [39] B. Strand. Summation by parts for finite difference approximations for d/dx . *J. Comput. Phys.*, 110:47–67, 1994.
- [40] David C Del Rey Fernández, Jason E Hicken, and David W Zingg. Review of summation-by-parts operators with simultaneous approximation terms for the numerical solution of partial differential equations. *Computers & Fluids*, 95:171–196, 2014.
- [41] Magnus Svärd and Jan Nordström. Review of summation-by-parts schemes for initial-boundary-value problems. *Journal of Computational Physics*, 268:17–38, 2014.
- [42] Gregor J Gassner. A skew-symmetric discontinuous galerkin spectral element discretization and its relation to sbp-sat finite difference methods. *SIAM Journal on Scientific Computing*, 35(3):A1233–A1253, 2013.
- [43] Mark A Taylor and Aimé Fournier. A compatible and conservative spectral element method on unstructured grids. *Journal of Computational Physics*, 229(17):5879–5895, 2010.
- [44] Kieran Ricardo, David Lee, and Kenneth Duru. Entropy and energy conservation for thermal atmospheric dynamics using mixed compatible finite elements. *Journal of Computational Physics*, 496:112605, 2024.
- [45] Kieran Ricardo, Kenneth Duru, and David Lee. An entropy stable discontinuous galerkin method for the spherical thermal shallow water equations. *SIAM Journal on Scientific Computing*, 46(6):A3353–A3374, 2024.
- [46] L. Dovgilevich and I. Sofronov. High-accuracy finite-difference schemes for solving elastodynamic problems in curvilinear coordinates within multi-block approach. *Appl. Numer. Math.*, 93:176–194, 2015.
- [47] Ken Mattsson. Diagonal-norm upwind sbp operators. *Journal of Computational Physics*, 335:283–310, 2017.
- [48] Christopher Williams and Kenneth Duru. Full-spectrum dispersion relation preserving summation-by-parts operators. *SIAM Journal on Numerical Analysis*, 62(4):1565–1588, 2024.
- [49] Hendrik Ranocha, Andrew R. Winters, Michael Schlottke-Lakemper, Philipp Öffner, Jan Glaubitz, and Gregor J. Gassner. On the robustness of high-order upwind summation-by-parts methods for nonlinear conservation laws. *Journal of Computational Physics*, 520:113471, 2025.
- [50] Lukas Lundgren and Ken Mattsson. An efficient finite difference method for the shallow water equations. *Journal of Computational Physics*, 422:109784, 2020.
- [51] Bertil Gustafsson, Heinz-Otto Kreiss, and Joseph Oliger. *Time dependent problems and difference methods*, volume 24. John Wiley & Sons, 1995.
- [52] Mark H Carpenter, David Gottlieb, and Saul Abarbanel. Time-stable boundary conditions for finite-difference schemes solving hyperbolic systems: methodology and application to high-order compact schemes. *Journal of Computational Physics*, 111(2):220–236, 1994.
- [53] *Boundary Treatment*, pages 127–156. Springer Berlin Heidelberg, Berlin, Heidelberg, 2008.
- [54] David Lee, Artur Palha, and Marc Gerritsma. Discrete conservation properties for shallow water flows using mixed mimetic spectral elements. *Journal of Computational Physics*, 357:282–304, 2018.
- [55] Bertil Gustafsson. The convergence rate for difference approximations to mixed initial boundary value problems. *Mathematics of Computation*, 29(130):396–406, 1975.
- [56] Bertil Gustafsson. The convergence rate for difference approximations to general mixed initial boundary value problems. *SINUM*, 18(2):179–190, 1981.
- [57] Magnus Svärd and Jan Nordström. On the order of accuracy for difference approximations of initial-boundary value problems. *J. Comput. Phys.*, 218(1):333–352, 2006.
- [58] Anders Szepessy. Convergence of a shock-capturing streamline diffusion finite element method for a scalar conservation law in two space dimensions. *Mathematics of Computation*, 53(188):527–545, 1989.
- [59] Jeff Bezanson, Alan Edelman, Stefan Karpinski, and Viral B Shah. Julia: A fresh approach to numerical computing. *SIAM Review*, 59(1):65–98, 2017.
- [60] Hendrik Ranocha. SummationByPartsOperators.jl: A Julia library of provably stable semidiscretization techniques with mimetic properties. *Journal of Open Source Software*, 6(64):3454, 08 2021.

- [61] Steven J. Ruuth. Global optimization of explicit strong-stability-preserving runge-kutta methods. *Mathematics of Computation*, 75(253):183–207, 2006.
- [62] Christopher Rackauckas and Qing Nie. Differentialequations.jl – a performant and feature-rich ecosystem for solving differential equations in julia. *The Journal of Open Research Software*, 5(1), 2017. Exported from <https://app.dimensions.ai> on 2019/05/05.
- [63] Simon Danisch and Julius Krumbiegel. Makie.jl: Flexible high-performance data visualization for Julia. *Journal of Open Source Software*, 6(65):3349, 2021.
- [64] James Paul Ahrens, Berk Geveci, and C. Charles Law. Paraview: An end-user tool for large-data visualization. In *The Visualization Handbook*, 2005.
- [65] Andrew TT McRae and Colin J Cotter. Energy-and enstrophy-conserving schemes for the shallow-water equations, based on mimetic finite elements. *Quarterly Journal of the Royal Meteorological Society*, 140(684):2223–2234, 2014.
- [66] Joseph Galewsky, Richard K Scott, and Lorenzo M Polvani. An initial-value problem for testing numerical models of the global shallow-water equations. *Tellus A: Dynamic Meteorology and Oceanography*, 56(5):429–440, 2004.
- [67] Pedro S Peixoto and Martin Schreiber. Semi-lagrangian exponential integration with application to the rotating shallow water equations. *SIAM Journal on Scientific Computing*, 41(5):B903–B928, 2019.
- [68] Olivier Delestre, Carine Lucas, Pierre-Antoine Ksinant, Frédéric Darboux, Christian Laguerre, T.-N.-Tuoi Vo, François James, and Stéphane Cordier. Swashes: a compilation of shallow water analytic solutions for hydraulic and environmental studies. *International Journal for Numerical Methods in Fluids*, 72(3):269–300, October 2012.
- [69] Chi-Wang Shu. *Essentially non-oscillatory and weighted essentially non-oscillatory schemes for hyperbolic conservation laws*, pages 325–432. Springer Berlin Heidelberg, Berlin, Heidelberg, 1998.